Asymptotic safety casts its shadow

Aaron Held,[a,1] **Roman Gold**[b] **and Astrid Eichhorn**[c,a]

[a]Institut für Theoretische Physik, Universität Heidelberg,
  Philosophenweg 16, 69120 Heidelberg, Germany
[b]Institut für Theoretische Physik, Johann Wolfgang Goethe-Universität,
  Max-von-Laue-Straße 1, 60438 Frankfurt, Germany
[c]CP3-Origins, University of Southern Denmark,
  Campusvej 55, DK-5230 Odense M, Denmark

E-mail: held@thphys.uni-heidelberg.de, gold@itp.uni-frankfurt.de,
eichhorn@sdu.dk

Abstract. We set out to bridge the gap between regular black-hole spacetimes and observations of a black-hole shadow by the Event Horizon Telescope. We explore modifications of spinning and non-spinning black-hole spacetimes inspired by asymptotically safe quantum gravity which features a scale dependence of the Newton coupling. As a consequence, the predictions of our model, such as the shadow shape and size, depend on one free parameter determining the curvature scale at which deviations from General Relativity set in. In more general new-physics settings, it can also depart substantially from the Planck scale. In this case, the free parameter is constrained by observations, since the corresponding curvature scale is significantly below the Planck-scale. The leading new-physics effect can be recast as a scale-dependent black-hole mass, resulting in distinct observational signatures of our model. As a concrete example, we show that two mass-measurements, extracted from the size of the shadow and from Keplerian orbital motion of stars, allow to distinguish the classical from the modified, regular black-hole spacetime, yielding a bound on the free parameter. For spinning black holes, we further find that the singularity-resolving new physics puts a characteristic dent in the shadow. Finally, we argue, based on the underlying physical mechanism, that the effects we derive could be generic consequences of a large class of quantum-gravity theories.

---

[1]Corresponding author.

Contents

1 Motivation

The true nature of black holes, either those located at essentially all centres of galaxies [34] or their stellar mass counterparts [122] is an exciting question that brings us to the limit of (if not beyond) our understanding of the inner workings of gravity. Quantum gravity is expected to strongly modify the geometry of spacetime in the interior of black holes, where classical solutions feature singularities. Quantum-gravity effects in black-hole spacetimes have been explored, e.g. in [11, 22, 24, 25, 67–70, 86, 89, 111, 112, 131, 134]. Moreover, proposals for singularity-free black-hole-like spacetimes have been made, e.g. in [17, 53, 54, 85]. In these cases, the metric is strongly modified close to the classical singularity, but effects can persist even outside the horizon.

The possibility to directly image a black hole with the technique of Radio Very-Long-Baseline-Interferometry [38–43, 51, 62] is an exciting and promising development in gravitational physics. Zooming in on the horizon, will there be detectable imprints of the fundamental quantum structure of spacetime? According to a standard power-counting argument such signatures are highly suppressed by a power of $M_{\rm Pl}/M$ where M is the mass of the black hole and $M_{\rm Pl}$ the Planck mass, at least for astrophysically plausible black holes with masses between several tens to several billion solar masses. So, the conservative answer would be "no". Yet, the possibility of quantum-gravity effects at the horizon has been raised, e.g. in [6, 44, 75, 76, 84]. In particular, for extended objects like black-hole horizons, a simple power-counting argument based on the *local* curvature might be misleading. Moreover, given that singularities plague black-hole spacetimes in General Relativity, some form of new physics must exist to resolve these, not necessarily being quantum gravity. This motivates us

to explore quantum-gravity inspired models while keeping the scale at which deviations from (General Relativity) GR set in as a free parameter. However, in order to confront theoretical models with the data, we first need to know what we are looking for. In the classical case, the image of a black hole has first been studied, e.g. in [18, 88, 104, 143]. To construct the quantum analogue, potential consequences of quantum gravity for the spacetime geometry close to the horizon have yet to be understood even qualitatively.

Game-changing detections of gravitational waves [1] and the groundbreaking observations of the first image of M87* by the EHT [38–43] now enable observational probes of the metrics of the most compact objects in our universe. This provides access to a completely different regime of gravity than the well-tested weak-field regime, e.g. in the solar system, where GR has been tested extensively [150]. In contrast, both the origin of the detected gravitational-wave signals as well as the radio-emission detected by the EHT lie in the strong-field regime, where curvature effects become significant. A clear prerequisite for tests of GR based on EHT observations, as advocated in [30, 45, 61, 92, 93, 95, 120, 121, 152], is the development of model-predictions from modifications of GR, some of which might be of quantum origin. Specifically, the observable we focus on is the shape and size of black-hole shadows, which has become visible in images of horizon-scale structures [38–43]. A black hole by itself does not emit any light — by construction. It also blocks a significant portion of light emitted behind the black hole. The resulting darkness contrasts against any otherwise bright background emission. Moreover, the strong bending of light rays by the black hole generates a luminous ring of light demarcating the shadow. The shape and size of the shadow can be calculated given a form of the metric describing the black-hole spacetime. Due to the no-hair theorem, the mass and spin of the black hole are the only two parameters determining shape and size of the shadow in GR. In this case, the black-hole shadow is nearly circular in shape even for rapidly spinning black holes [120]. In alternative theories of gravity, richer structures are possible [31, 32, 94]. Shadows in modified theories of gravity have been studied for Chern-Simons gravity [7, 115], in Randall-Sundrum-type braneworld models [8] (also with cosmological constant [60]), in Scalar-Tensor-Vector-Gravity [109, 145] and tensor-vector gravity [140], Einstein-dilaton-Gauss-Bonnet gravity [14, 47], Einstein-Maxwell-dilaton-axion gravity [146], Einstein-Born-Infeld gravity [13] and conformal gravity [110]. Further, the shadows of super-extremal Kerr black holes [16] and Kerr-Newman-NUT spacetimes [83] as well as Kerr black holes with scalar hair [46, 142] have been explored. Regular spacetimes have been studied in [3, 9, 133, 138]. The shadow of non-commutative-geometry inspired black-hole spacetimes has been investigated in [147]. As an alternative to separate studies within distinct gravity theories, one can parameterise a more general metric than the Kerr metric, providing a way to constrain more than one theory of gravity at the same time [91, 100, 130, 152]. For actual comparisons with EHT observations, it is necessary to realistically model the dynamics of infalling matter, e.g. using GRMHD simulations [107].

Until now, no such predictions from asymptotically safe gravity [123, 149] are available and we set out to close this gap. The theory is based on the well-tested quantum-field theory framework which can successfully describe the three other fundamental interactions of nature, and extends it to include gravity. Further, it respects the observational evidence that the gravitational dynamics can be formulated purely in terms of the metric field by promoting the metric to a fundamental quantum field. Motivated by this conservative nature of asymptotically safe gravity, we explore asymptotic-safety inspired black-hole spacetimes to derive shape and size of the black-hole shadow. The key idea explored in this work consists in the onset of quantum-gravity effects and resulting modifications of the spacetime

at large curvature scales. As one might expect, Planck-scale modifications of GR cannot be constrained by the EHT observations.

While the specific black-hole spacetimes we analyse are motivated by an approach to quantum gravity, we take a broader view in which the modifications of GR are not necessarily tied to the Planck scale. Remaining agnostic about the type of new physics that sources the singularity-resolving modifications, we derive bounds on the new parameter determining the size of the deviations from GR.

This paper is structured as follows. We provide an introduction to asymptotically safe quantum gravity and explain how to set up asymptotic-safety inspired black-hole spacetimes in the spherically symmetric and axisymmetric case in section 2. We review how to calculate the shadow of a black hole in section 3 and present our results in section 4, where we also interpret the physical mechanism underlying the resulting deformation of the shadow compared to the classical case. We further broaden our view beyond quantum gravity as the new physics that leads to singularity resolution and explain how to constrain a wider parameter space in our model. In section 5, we summarise our key findings and argue that qualitatively similar effects could be a generic consequence of a large class of quantum-gravity theories.

2 Black holes in asymptotically safe gravity

Quantum fluctuations of spacetime result in a scale-dependence of the gravitational interactions. Thus, unlike in classical gravity, the Newton coupling is not a simple constant, but changes as a function of scale due to the impact of quantum fluctuations, just like the other fundamental interactions of nature "run" as a consequence of quantum fluctuations, (as for instance in QCD). In quantum field theories, such a scale dependence can terminate in an unphysical infinity, a so-called Landau pole, which implies a breakdown of the quantum-field theoretic description at the corresponding finite scale and requires some form of new physics. Under one condition, such poles can be avoided, rendering the quantum field theory a viable description up to arbitrarily microscopic scales. This condition consists in an enhanced symmetry, namely quantum scale-invariance: in such a scale-invariant regime, the dynamics do not depend on the scale, allowing one to zoom in up to arbitrarily small scales without running into any inconsistencies. The simplest form of quantum scale invariance is asymptotic freedom, which consists in the absence of interactions in the microscopic regime. While it plays a central role for the Standard Model of particle physics, asymptotic freedom cannot be achieved in quantised GR due to its infamous perturbative nonrenormalisability [80, 135, 139]. Historically, this result led to the development of alternative descriptions of quantum gravity, including, e.g. string theory and loop quantum gravity. Yet, just as for other fundamental interactions, an alternative to asymptotic freedom could exist also for a quantum field theory of the metric, namely asymptotic safety. In an asymptotically safe setting, dimensionless coupling strengths become constant beyond the transition scale to the scale-invariant regime, realising quantum scale invariance in the presence of residual interactions. For dimensionful interaction strengths, such as the Newton coupling, quantum scale-invariance implies that they scale canonically with the Renormalisation Group (RG) scale k. This ensures that the dimensionless counterpart of these interactions (constructed by multiplication with appropriate powers of k, is constant instead of changing with k) just as it has to be in a scale-invariant setting, see eq. (2.1) for the Newton coupling.

Thus, the key idea of asymptotically safe gravity [149] is that quantum scale-symmetry holds beyond a microscopic transition scale, typically assumed to be the Planck scale. This

requires quantum fluctuations to be antiscreening, such that the dimensionless counterpart of the Newton coupling becomes constant beyond the Planck scale, $g(k) = G_N(k)k^2 = \text{const}$. For the dimensionful Newton coupling, the antiscreening by quantum-gravity fluctuations results in a fall-off

$$G_N(k) = \frac{g_*}{k^2}, \tag{2.1}$$

beyond the transition scale to the fixed-point regime. Herein g_* is the asymptotically safe fixed-point value. A consequence of eq. (2.1) is an effective weakening of gravity in the far ultraviolet. Heuristically, this is just what one would expect for a quantum theory of gravity that is capable of resolving the singularities present in classical gravity.

Compelling indications for the existence of an asymptotically safe regime in quantum gravity have been found [19, 21, 36, 37, 52, 59, 63, 66, 77, 101, 102, 124], see [117, 127] for introductions. Unexpected potential implications for particle-physics phenomenology have been found in [57, 58, 132], for recent reviews containing a discussion of open questions see [55, 56].

The full dynamics of gravity in the far UV in asymptotic safety includes terms beyond the Einstein-Hilbert action [21, 36, 66, 77]. For the purposes of our paper, we will limit ourselves to a simplified setting and explore the scale-dependence of the Newton coupling for black-hole spacetimes as an expected leading-order effect of asymptotically safe gravity. The effect of a cosmological constant has been explored in [5, 97, 98, 116], where an RG improvement considering a canonical scaling of the cosmological constant in the fixed-point regime leads to the reintroduction of a singularity. Yet, an IR value of the cosmological constant, as required by cosmological observations, is compatible with a vanishing fixed-point value, such that the cosmological constant might not play a role for the structure of the black-hole spacetime in the vicinity of the classical singularity, as analysed in [5]. We follow [5] in constructing RG-improved Schwarzschild and Kerr spacetimes and treat the cosmological constant as an IR scale that can be neglected in our setting. The impact of higher-order curvature terms, as expected from asymptotic safety, on the black-hole shadow will be studied elsewhere [87]. In exploring the impact of a scale-dependent Newton coupling on black-hole shadows, we make the key assumption that those indications for asymptotic safety in gravity collected in the Riemannian regime (with the exception of [105]) are applicable to the Lorentzian regime.

To upgrade the classical black-hole spacetimes to modified, "asymptotic-safety inspired" black-hole spacetimes, we focus on the scale dependence of the Newton coupling, generated by quantum fluctuations

$$G_N(k) = \frac{G_0}{1 + \gamma\, G_0 k^2}. \tag{2.2}$$

Here, G_0 is the classical value of the Newton coupling, and $\gamma > 0$ is the inverse dimensionless fixed-point value ($\gamma = g_*^{-1}$), i.e. the square of the inverse transition scale to the fixed-point regime, measured in Planck units. In a simple approximation, the scale comes out as roughly the Planck scale, but upgrades including the impact of quantum-fluctuations of matter show that γ^{-1} can vary [52]. k is the Renormalisation Group scale, i.e. an energy scale that can loosely be interpreted as the inverse resolution scale of the theory: for low k, one probes the classical regime of the theory, whereas one enters the quantum regime for $k^2 G_0 > \gamma^{-1}$. In other words, γ^{-1} is the transition scale to the quantum regime in units of the classical Planck mass, cf. figure 1. For the remainder of this paper, we treat γ as a free parameter.

Hints that the fall-off of the Newton coupling due to antiscreening quantum fluctuations in the UV could indeed lead to singularity-free black-hole spacetimes have been found
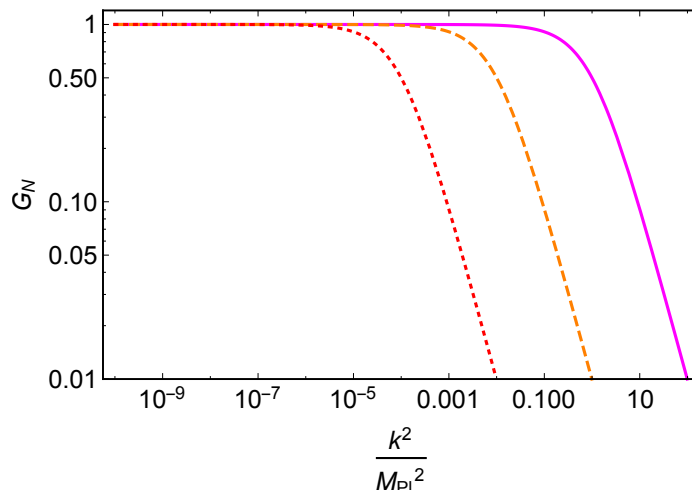
Figure 1. Running Newton coupling in units of the classical Planck mass for $\gamma = 1$ (continuous magenta line), $\gamma = 10^2$ (orange dashed line) and $\gamma = 10^4$ (red dotted line). The classical regime with $G_N = \text{const}$ and the quantum regime with $G_N \sim k^{-2}$ are separated by the transition scale $\gamma^{-1} M_{\text{Pl}}$.

in [5, 24–29, 64, 65, 97–99, 103, 116, 118, 136, 137]. In these works, the key idea is to investigate an effective metric that should be understood as the expectation value of the metric in the quantum theory. Starting from the classical metric, e.g. Schwarzschild or Kerr, the RG-improved metric is constructed following two steps. Firstly, the Newton coupling in the metric is replaced by its scale-dependent counterpart which encodes the effect of quantum fluctuations of gravity. Secondly, the Renormalisation Group scale k that the Newton coupling depends on is identified with a physical scale of the classical spacetime. This results in a modified metric, which is a solution to the Einstein equations with an effective energy-momentum tensor. The interpretation of the latter is that it encodes the quantum-gravity contributions at an effective level.

We stress that this procedure it not a strict derivation from asymptotically safe gravity. Instead, it makes two crucial assumptions: (i) The full dynamics of the theory is truncated to an Einstein-Hilbert term. (ii) Quantum effects are included by taking into account the RG scale dependence of the Newton coupling, and making the assumption that a physical scale of a classical black-hole spacetime can be identified with the RG scale. Overall this results in asymptotic-safety inspired models for regular black-hole spacetimes.

2.1 Improved Schwarzschild spacetime

To upgrade the classical solution by the quantum-induced scale dependence, we identify k with the curvature scale to some appropriate power. For the classical Schwarzschild case, the Kretschmann scalar is

$$K = \frac{48 G_0^2 M^2}{r^6}. \tag{2.3}$$

On dimensional grounds, we choose

$$k^2 = \alpha K^{\frac{1}{2}}, \tag{2.4}$$

with a dimensionless α of order one. It is convenient to choose $\alpha = 48^{-1/2}$ (such choices can be reabsorbed in the free parameter γ), such that

$$k^2 = \frac{MG_0}{r^3}. \tag{2.5}$$

This results in the following "upgraded" line element

$$ds^2 = -f(r)dt^2 + f(r)^{-1}dr^2 + r^2 d\Omega^2, \tag{2.6}$$

with

$$f(r) = 1 - 2M\frac{G_N(r)}{r} = 1 - \frac{2M}{r\,M_{\rm Pl}^2}\frac{1}{1 + \gamma\left(\frac{M}{M_{\rm pl}^4 r^3}\right)}, \tag{2.7}$$

where we have set $G_0 = M_{\rm Pl}^{-2}$ in the second step, i.e. we work in natural units. Due to the scale-dependence of G_N, working in units with $G_0 = 1$, as typically done in GR, is not suited to our setting. In natural units the gravitational radius is given by $r_g = M/M_{\rm Pl}^2$. We measure all radial distances in units of r_g.

Further, we absorb a factor of M^2 defining

$$\tilde{\gamma} = \frac{\gamma\,M_{\rm Pl}^2}{M^2}. \tag{2.8}$$

By working with $\tilde{\gamma}$, all our results apply to arbitrary ratios of $M/M_{\rm Pl}$. Here, we already anticipate that in a more general new-physics setting, one possibly needs to explore significantly larger γ.

With these definitions, the function $f(r)$ in the line element simplifies to

$$f(r) = 1 - \frac{2\,r^2/r_g^2}{r^3/r_g^3 + \tilde{\gamma}}\,. \tag{2.9}$$

Note that the corresponding spacetime is regular and retains a horizon whose location is given by

$$r_H/r_g = \frac{1}{6}\left[4 + \frac{8\times2^{1/3}}{\left(16 - 27\tilde{\gamma} + 3\sqrt{3\tilde{\gamma}^2(-32 + 27\tilde{\gamma})}\right)^{1/3}} + 2^{2/3}\left(16 - 27\tilde{\gamma} + 3\sqrt{3\tilde{\gamma}^2(-32 + 27\tilde{\gamma})}\right)^{1/3}\right]. \tag{2.10}$$

In the limit $\tilde{\gamma} \to 0$, where the modifications are switched off, r_H approaches the value of the Schwarzschild solution, $r_H \to 2\,r_g$, as expected. In particular, this limit is approached for $M \gg M_{\rm Pl}$ at fixed γ. The horizon shrinks as $\tilde{\gamma}$ is increased, cf. figure 2. For all $\tilde{\gamma}$, the quantum-gravity inspired black-hole solution has a smaller horizon than its classical counterpart. The difference becomes more pronounced as γ is increased, i.e. the onset of quantum-gravity effects is pushed towards lower curvature scales.

The RG-improved line element takes a de-Sitter-like form for small r, implying a second zero of $f(r)$ below the outer horizon. As $\tilde{\gamma}$ is increased, the two zeros of $f(r)$ move toward each other and annihilate at a critical $\tilde{\gamma}_{\rm crit} = 32/27$, such that the remaining object no longer features a horizon [25]. For the remainder of this paper, we focus on smaller values of $\tilde{\gamma} < \tilde{\gamma}_{\rm crit}$, where no such drastic modification of the causal structure of the spacetime occurs.
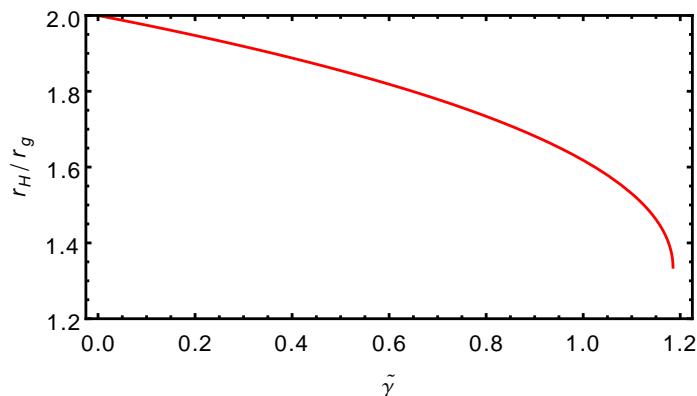
Figure 2. We show the radial coordinate of the horizon as a function of $\tilde{\gamma}$, see eq. (2.10).

In appendix B we discuss additional features of the shadow in the axisymmetric spacetime, which occur just before the horizon disappears. For even larger spin or larger $\tilde{\gamma}$ the horizon disappears and leaves behind a horizonless compact object. Understanding simulated EHT-images for such horizonless spacetimes is an intriguing future question that is beyond the scope of this work.

2.2 Improved Kerr spacetime

Astrophysically, black holes (supermassive or stellar-mass ones) are formed in non-spherical systems, either from rotating gas clouds, binary mergers, or violently exploding massive stars. Observationally, there is growing evidence for non-zero black-hole spin as indicated, e.g. by measurements of the $Fe\,K\alpha$ emission line profiles [128, 129]. Independently, the recent LIGO detections [1, 2] of GWs strongly favour black holes with non-zero spin. More generally, even if two merging black holes had vanishing initial spins, they would form a Kerr black hole of spin $a \sim 0.69\, r_g$ [119]. Moreover, one of the leading models to explain jet formation, the Blandford-Znajek mechanism [23] demands non-zero black-hole spin and fuels the jets by energy extraction from the ergosphere via magnetic fields. Finally, the EHT observations in conjunction with the jet-power estimates provide indications for a non-zero spin of M87* [42].

This strongly motivates us to take a step beyond spherical symmetry, and consider the asymptotic-safety inspired upgrade of the Kerr spacetime. The classical line element in Boyer-Lindquist coordinates is given by

$$ds^2 = -\frac{\Delta_r - a^2 \sin(\theta)^2}{\rho^2}\, dt^2 + \frac{\rho^2}{\Delta_r}\, dr^2 + \rho^2\, d\theta^2 + \frac{(a^2 + r^2)^2 - a^2\, \Delta_r\, \sin(\theta)^2}{\rho^2}\, \sin(\theta)^2\, d\phi^2$$
$$- \frac{2(a^2 + r^2 - \Delta_r)}{\rho^2} a\, \sin(\theta)^2\, dt\, d\phi\,. \tag{2.11}$$

Herein, the specific angular momentum is given by $a = J/M$ and lies between 0 and r_g. Further, we use

$$\rho^2 = r^2 + a^2 \cos^2\theta, \tag{2.12}$$
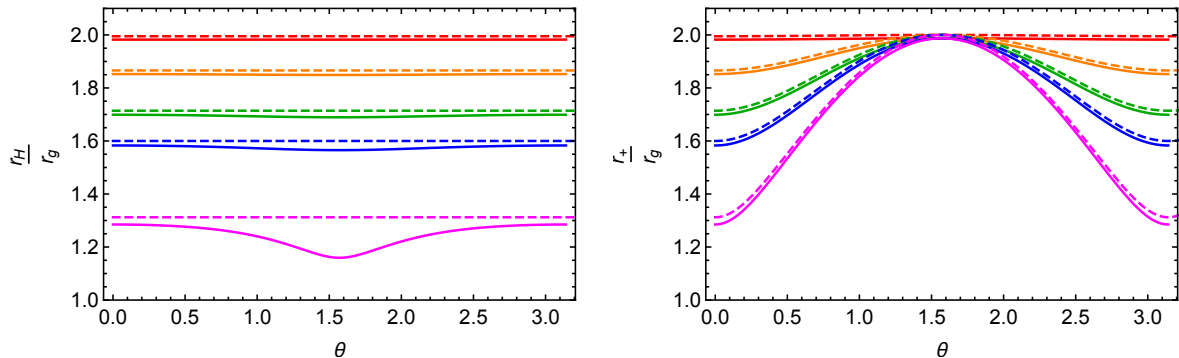$$\Delta_r = r^2 + a^2 - 2G_N\, M\, r. \tag{2.13}$$

Figure 3. Left panel: we show the classical location of the outer horizon (dashed lines) and the quantum-improved case (continuous lines) for $\gamma = 0.05$ from top to bottom for $a = 0.\,r_g$ (red), $a = 0.5\,r_g$ (orange), $a = 0.7\,r_g$ (green), $a = 0.8\,r_g$ (blue) and $a = 0.95\,r_g$ (magenta). Right panel: location of the outer boundary of the ergoregion in the same cases.

The corresponding classical Kretschmann scalar which forms the basis for our scale identification takes the form

$$K(r,\theta,a) = \frac{48 G_0^2 M^2}{(r^2 + a^2 \cos(\theta)^2)^6} \Big(r^6 - 15 r^4 a^2 \cos(\theta)^2 + 15 r^2 a^4 \cos(\theta)^4 - a^6 \cos(\theta)^6 \Big). \quad (2.14)$$

To date, all RG improvements of the Kerr solution have used a spherically symmetric scale identification [103, 116, 125, 126]. Yet the curvature actually only diverges in the equatorial plane, and accordingly grows in a θ-dependent fashion, as one approaches the singularity. This suggests that singularity-resolving quantum effects should be strongest in the equatorial plane. Our curvature-informed RG improvement will therefore exhibit an angular dependence, in addition to the radial dependence, as in the Schwarzschild case. Intuitively speaking, ingoing geodesics at different angles thus differ in their sensitivity to quantum effects.

Following a dimensional argument, we would again identify

$$k^2 = \alpha\, K(r,\theta,a)^{\frac{1}{2}}, \quad (2.15)$$

and choose $\alpha = 48^{-1/2}$ for simplicity. However, it is crucial to note that for specific values of a and θ, the Kretschmann scalar K becomes negative, even outside the horizon. This would result in an imaginary, and therefore unphysical k^2. On the other hand, one would expect only the magnitude of K to set the relevant scale. This motivates our RG-improvement of the form

$$k^2 = \frac{G_0 M}{(r^2 + a^2 \cos(\theta)^2)^3} r^3, \quad (2.16)$$

which corresponds to an identification with the main fraction in the Kretschmann scalar eq. (2.14), neglecting the θ-dependent polynomial. The RG-improved metric outside the horizon takes the form eq. (2.11) with $G_N(k^2)$ and k^2 as in eq. (2.16). As a consequence of the RG improvement, the black-hole spacetime is regular. The RG-improved axisymmetric spacetime reduces to its spherically symmetric counterpart for $a \to 0$, as it should.

As in the Schwarzschild case, the horizon lies at lower values of r. Additionally, it exhibits a θ-dependence that becomes more pronounced as the deviation from spherical symmetry grows, i.e. as a is increased, cf. upper panel of figure 3. Due to the fall-off of the RG-improvement effect with radial distance, the modification to the boundary of the ergoregion is smaller, cf. lower panel of figure 3. As a consequence, the ergoregion for the RG improved black-hole spacetime is slightly larger in volume than in the classical case.

3 Methods

Generating an image of the horizon as seen by a distant observer requires tracing light rays through the corresponding black-hole geometry. Pioneering first approaches evolved geodesics forward in time from source to observer and considered radiative transfer from optically thick, geometrically thin accretion disks [18, 48]. [104] first traced geodesics backwards in time from observer to source, which, in the case of homogeneous and non-localised sources, is far more efficient for a typically very localised observer. We will use similar techniques here. More recently, efficient methods [20, 141] for ray tracing involving both a localised source and localised observer have also been developed.

3.1 Geodesic equation

In a given spacetime the trajectories of light rays are governed by the null geodesic equation

$$\frac{d^2 x^\rho}{d\lambda^2} = -\Gamma^\rho_{\mu\nu} \frac{dx^\mu}{d\lambda} \frac{dx^\nu}{d\lambda} \,, \tag{3.1}$$

where x^ρ is the position of the photon; λ is an affine parameter parameterising the photon's world line; and $\Gamma^\rho_{\mu\nu}$ is the metric-compatible Christoffel connection. We implement the geodesic equation (3.1) as eight coupled first-order ordinary differential equations

$$\frac{dx^\rho}{d\lambda} = k^\rho \,, \quad \frac{dk^\rho}{d\lambda} = -\Gamma^\rho_{\mu\nu} \, k^\mu \, k^\nu \,. \tag{3.2}$$

For the purpose of this paper, $\Gamma^\rho_{\mu\nu}$ are given in analytical form and since computation time is not critical, we use the native numerical integration techniques available in Mathematica [151].

3.2 Camera setup & image

We position a distant virtual camera far away from the black hole where the geometry is well-approximated by flat spacetime. We will optimise this distance with respect to precision and computation time in the following section. The coordinates of the origin of the image plane in Boyer-Lindquist coordinates are given by $(r_{\text{cam}}, i, \phi_{\text{cam}})$. The image plane itself is spanned by two Cartesian coordinates (x, y). Each point in this image plane can be expressed in Boyer-Lindquist coordinates (r, θ, ϕ) of the black-hole spacetime by the following transformation

$$r^2 = \sigma + \sqrt{(\sigma^2 + a^2 \, Z^2)^{1/2}} \,, \; \cos\theta = Z/r \,, \; \tan\phi = Y/X \,, \tag{3.3}$$

where $\sigma = \left(X^2 + Y^2 + Z^2 - a^2 \right)/2$. Here, (X, Y, Z) are Cartesian coordinates centred around the black hole. They are in turn related to the image coordinates (x, y) by

$$X = \mathcal{D} \cos\phi_{\text{cam}} - x \sin\phi_{\text{cam}} \,, \tag{3.4}$$

$$Y = \mathcal{D} \sin\phi_{\text{cam}} + x \cos\phi_{\text{cam}} \,, \tag{3.5}$$

$$Z = r_{\text{cam}} \cos(i) + y \sin(i) \,, \tag{3.6}$$

where $\mathcal{D} = \sin(i)\sqrt{r_{\text{cam}}^2 + a^2} - y \cos(i)$.

All the light rays are initialised perpendicular to the screen in which case their initial momentum vector can be calculated by differentiating eqs. (3.3).

We parameterise the shadow boundary in the $x - y$ image plane by its radial distance from the origin $\rho(\psi)$ in the image plane as a function of the angle ψ between the x-Axis and the radial vector, cf. figure 7. The resulting shadow boundary is determined by bisecting nested radial intervals for each ψ: depending on whether the light ray crosses the horizon (and metric components in Boyer-Lindquist coordinates diverge), or escapes to large radii, the outer or inner interval is chosen for the next iteration.

To obtain the intensity distribution generated by a homogeneous background source, we employ the affine-parameter emissivity approximation [50]. We normalise the resulting intensity to the image point with the smallest affine parameter.

3.3 Error control

We use the deflection angle ϑ in the equatorial plane as a benchmark value for our error control. In classical Kerr spacetime this angle can be obtained from an analytical form with arbitrary precision [90]. In controlling the initial-data error, the discretisation error (due to a finite stepsize), and the computational errors due to finite numerical precision, we rely on standardised and well-known error control of the native ODE-solver, i.e. [151].

Additionally, there is an error due to the finite radial camera distance. At large distance $r_{\text{cam}} \gg r_g$ all investigated black-hole metrics converge to flat space. In this regime, the dependence of the deflection angle ϑ on the radial distance is therefore expected to obey the functional form

$$\vartheta_{\text{fit}}(r_{\text{cam}}) = \vartheta_0 - b/r_{\text{cam}}. \tag{3.7}$$

We fit this function to a series of data points obtained at increasing values of r_{cam} to determine the parameters ϑ_0 and b. Specifying a chosen maximal error $\Delta\vartheta = \vartheta_{\text{fit}}(r_{\text{cam}}) - \vartheta_0$ determines the required radial distance $r_{\text{cam}}(\Delta\vartheta)$. In appendix A, we apply this procedure to fit the exact known result for Kerr spacetime. The exact form for θ in the equatorial plane allows us to also benchmark the required numerical precision. In appendix A, we also demonstrate the radial distance error control for an explicit deflection angle in the equatorial plane of the RG-improved spacetime.

Kerr-like spacetimes exhibit three constants of motion: the energy E, the angular momentum along the black-hole rotation axis L_Z, and the celebrated Carter constant $\mathcal{Q}$ [33]. We use the conservation of energy and the angular momentum as independent checks of our numerical error.

4 Results

We have motivated the RG-improved metrics for the spherically symmetric and axisymmetric case from asymptotically safe gravity. Yet, quantum gravity is just one specific candidate for new physics leading to singularity resolution. From a more agnostic point of view, the study of singularity-free, black-hole like geometries should proceed from a vantage point independent of one specific theory. In the present context, this implies that the parameter γ is not required to be close to 1, as the scale where modifications set in need not be tied to the Planck scale. Thus, it is of interest to constrain the resulting, large parameter space which can most efficiently be done by strong-field observations. Working with $\tilde{\gamma}$ instead of the original parameter γ allows us to investigate the modifications to shape and size of the shadow in a black-hole mass-independent fashion, as $\tilde{\gamma}$ scales appropriately with M, whereas the magnitude of the effect decreases at fixed γ as M is increased.
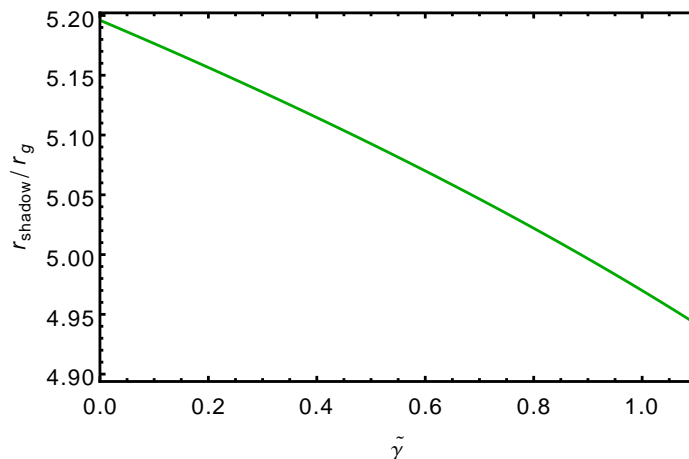
Figure 4. Coordinate location of the shadow for the spherically symmetric spacetime as a function of $\tilde{\gamma}$. The classical case is $\tilde{\gamma} = 0$.

4.1 Spherically symmetric black-hole spacetimes and their shadows

We first focus on the spherically symmetric case. We observe that the size of the shadow decreases as a function of $\tilde{\gamma}$, cf. figure 4. Intuitively, this is to be expected: in our setting, quantum-gravity effects lead to a weakening of the gravitational interaction strength. At a given proper distance to the centre of the black hole, the escape velocity is lowered compared to the classical case, as an observer leaving the black hole in their rocket experiences less gravitational pull in the quantum-improved case. Therefore, the "point of no return" for any infalling observer lies closer to the centre. Accordingly, weaker gravity leads to a more compact event horizon.

The modifications of the spacetime resemble that of a classical Schwarzschild black hole of lower mass. This begs the question whether there is a degeneracy between the classical Schwarzschild solution of mass M and the RG-improved solution of mass $M' < M$. Indeed, this is the case if the size of the shadow is the only observable that is accessible. Yet, a comparison of the intensity distributions in the two cases already demonstrates that there are additional differences, cf. figure 5.

The modifications due to RG improvement are *not* a simple rescaling of a classical Schwarzschild solution in the form $M \to M'$. Specifically, one can rewrite the RG-improved metric in the form of the classical Schwarzschild metric with an *effective* mass that depends on the radial distance, obtained by rearranging eq. (2.7),

$$M_{\mathrm{eff}}(r) = \frac{M}{1 + \tilde{\gamma} \left(\frac{r_g}{r}\right)^3}. \tag{4.1}$$

At the horizon, the difference between $M_{\mathrm{eff}}(r)$ and M is largest, and the modifications fall off with r^{-3}. This highlights that the deviation from classical Schwarzschild that we explore is a strong-field effect: while the deviation is at the level of about 10% close to the horizon (for $\tilde{\gamma} \approx 1$), it falls off rapidly with increasing radius.

The classical Schwarzschild spacetime and the RG-improved case can be distinguished via the r-dependence in eq. (4.1). Specifically, one can in principle extract the effective mass at two different distances from the black hole. For instance, one measurement can be
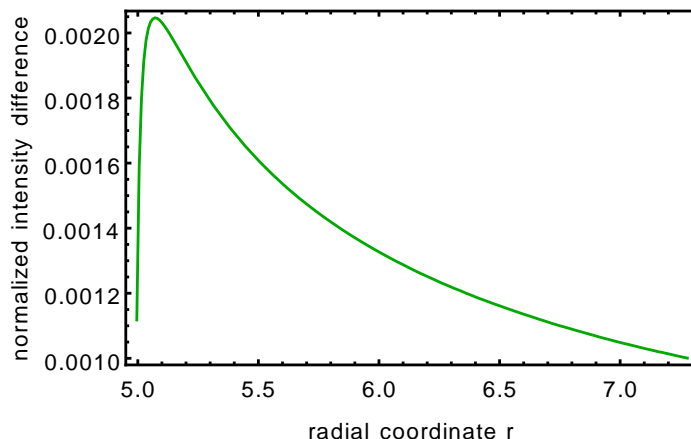
Figure 5. Relative intensity difference (within the approximate emissivity scheme) as a function of r, in units of r_g, between the RG improved black-hole spacetime and classical Schwarzschild spacetime with $M' < M$, such that both feature the same shadow size.

extracted from the size of the shadow at distances $\sim M$. The second could use the Keplerian orbital periods of nearby stars at distances of $\gtrsim 10^3 M$ (e.g. the pericentre distance of the star S2 in the galactic centre [72, 73, 78, 106]). Weighing black holes using the orbital motion of nearby stars is still possible, even for spatially unresolved orbital motion, via spectral analysis of emission line profiles of stars or gas in orbit around a supermassive black hole, as done for M87 [71, 144]. For a classical Schwarzschild spacetime, these results should agree. In the RG-improved case, the effective mass extracted from the size of the shadow is smaller than the effective mass extracted at larger radii (for small γ, i.e. effects tied to the Planck scale, only marginally so). This makes it evident that the modifications of the spacetime are not degenerate with a classical spherically symmetric spacetime.

For the case of M87*, the combined statistical and systematic error on the mass measured by the EHT collaboration is roughly 14 % [43]. Stellar-dynamics measurements yield an error of below 10 % [71], while gas dynamics observations have a significantly higher error [144] (note that these results are not in agreement with each other). Assuming that the near-horizon and far-horizon measurements should differ by one σ, these accuracies can be used to constrain $\tilde{\gamma} \lesssim 2$. Converted into γ, the higher mass of M87* compared to Sgr A* results in $\gamma \lesssim 2 \cdot 10^{95}$. This result highlights that modifications tied to the Planck scale will not be accessible by EHT observations. However, non-quantum, singularity-resolving gravitational physics might very well exist, and EHT observations do provide a way of probing or constraining the corresponding effects. We also highlight that the constraint $\tilde{\gamma} < 2$ cannot yet exclude horizon-less objects described by our RG improved metric. Future observations at higher frequencies and/or in polarization data, see [79] can result in tighter constraints, potentially ruling out horizonless objects in our setting.

Our result motivate a closer look at Sgr A*, given that at fixed $\tilde{\gamma}$, every order of magnitude in the mass corresponds to two orders of magnitude in the constraint on γ.

For Sgr A*, weak-field mass measurements come from tracking the orbital motion of stars around Sgr A* [4, 10, 35, 78, 81, 82]. The most recent result provides an accuracy of 0.3%, cf. [4]. Furthermore, let us assume that in the future, EHT will provide a measurement of the shadow size of Sgr A* with an accuracy of about 6 %, see [95]. In our model, these two measurements are expected to differ by one sigma for $\tilde{\gamma} \gtrsim 0.5$. Reinstating the black-hole

mass explicitly, this still translates into a constraint of $\gamma \lesssim 10^{89}$. We emphasize again, that this extraordinarily large number is a consequence of theoretical bias that the scale of new physics should be the Planck scale. Note that the scale of new physics is actually unknown, and therefore any constraint on the parameter space is important to achieve. Of course, if we use a different scale than $M_{\rm Pl}$ as our reference scale, the corresponding expected values for γ can increase dramatically, closing the gap to the observational constraints.

Stronger constraints will be possible if stars on tighter orbits than S2 are found and especially when a pulsar in orbit around a SMBH is found, as studied in [49]. Further, observations of the stellar dynamics making use of a forthcoming 39-m telescope are expected to provide a measurement of the black-hole mass with an accuracy of 0.1% [148]. Specifically, constraints $\tilde{\gamma} \sim \mathcal{O}(10^{-1})$ would become available if both measurements could reach a sub-percent accuracy. In particular, future observations of Sgr A* will thus probe values below $\tilde{\gamma}_{\rm crit}$ and distinguish horizon-less objects from black-hole spacetimes within our setting.

Let us contrast our results with observations in the weak-field regime. The gravitational parameter space can be spanned by two parameters, measuring the curvature ξ (given by the Kretschmann scalar for Schwarzschild) and the Newtonian potential ε (linked to an observable, namely the gravitational redshift). The highest curvatures probed in controlled laboratory experiments at low Newtonian potential are actually tests of the Newtonian inverse-square law, see, e.g. figure 2 in [15]. Specifically, following this reference, the absence of modifications to the inverse square law down to $56\,\mu m$ reached in [96] corresponds to a probe at $\xi = 6 \cdot 10^{-24} m^{-2}$. This should be contrasted with $\xi \approx 10^{-20} m^{-2}$ near the horizon of Sgr A*. Moreover, we highlight the following point: while tests of the inverse-square law proceed at very small $\varepsilon \approx 10^{-33}$ (see [15]), the EHT is sensitive to sources with $\varepsilon \approx 10^{-1}$. In the presence of a second scale, set by ε, an RG-improvement $\sim \varepsilon\,\xi$ could also be motivated. Accordingly, the strong-field regime should provide a qualitatively different test of the effects we propose here.

Beyond the specific model we explore here, we expect that the signature of quantum gravity we find here could be generic for a large class of quantum-gravity theories. For quantum-gravity effects to resolve the classical singularity, an effective weakening of gravity at high curvature scales — linked to an effective repulsive force from quantum gravity — is generically expected. This would imply, that quantum-improved black-hole horizons are more compact than their classical counterparts. The shrinking of the horizon (and consequently the shadow) through quantum-gravity effects can also be understood as a consequence of demanding a de-Sitter-like core in which the classical singularity is resolved. Inspecting the line element, we observe that a transition from Schwarzschild behaviour at asymptotically large distances to de-Sitter-like behaviour in the core requires a second zero of the function $f(r)$ in eq. (2.6). This results in a shift of the horizon to smaller values of r. Accordingly, we conjecture that most (if not all) quantum-gravity models will feature a (typically not large enough to be observable) signature of the form we discussed here, namely a more compact black-hole horizon and shadow. This can be reproduced by changing the one free parameter of the classical Schwarzschild solution, the mass, to a smaller value. The difference between physically different quantum theories of gravity lies in the fall-off of the effective mass, which could be different powers for different theories. Accordingly, a third mass-measurement at an intermediate distance could in principle distinguish these different theories. In practice, such differences are of course tiny, unless the curvature scale at which quantum-gravity effects set in is rather low. Remaining more agnostic about the type of new physics that leads to singularity resolution, the effective description in terms of a repulsive force (decreased black-
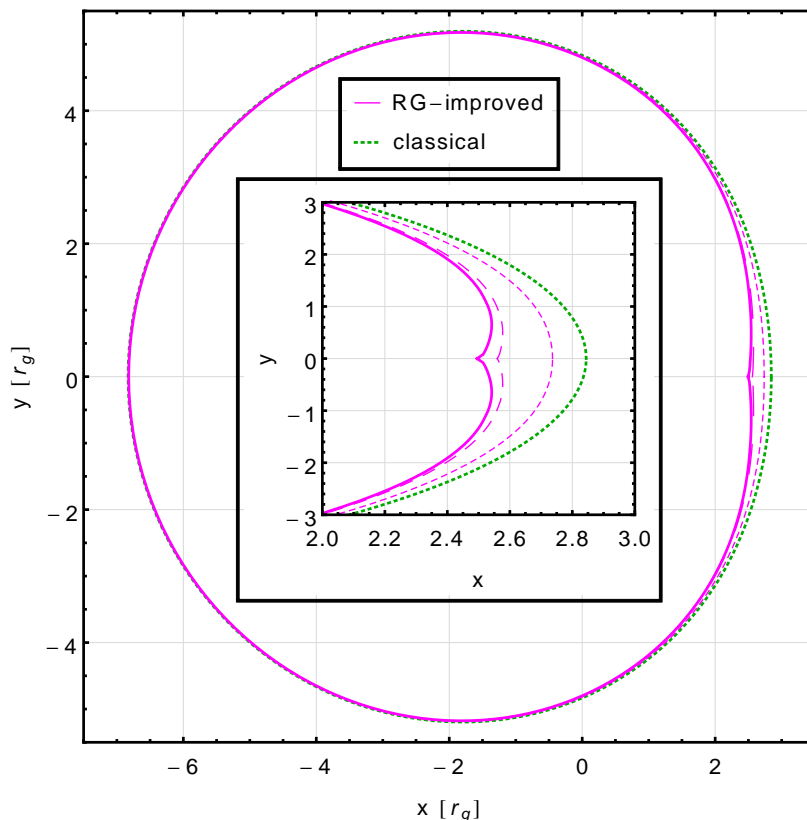
Figure 6. Classical Kerr shadow (green dotted) for $a = 0.9\,r_g$ and RG-improved case (magenta) for $a = 0.9\,r_g$. Growing values for $\tilde{\gamma} = (0.05, 0.1, 0.11)$ are indicated by smaller to larger dashing, respectively.

hole mass) remains well-motivated, with $\tilde{\gamma} \sim \mathcal{O}(1)$ not excluded. This calls for dedicated efforts to understand the dynamics of infalling and radiating matter in such spacetimes, in order to bridge the gap to actual EHT-images.

4.2 Axisymmetric black-hole spacetimes and their shadows

At leading order, the asymptotic-safety inspired effect is the same in the spherically symmetric and axisymmetric case, and consists in a reduced size of the shadow compared to the classical case, see figure 6. As a consequence of frame-dragging, rays that end up in the prograde (right) side of the image pass significantly closer to the horizon than those in the retrograde (left) side of the image. Accordingly, they pass through a regime of larger curvature, where the differences of the RG-improved and the classical spacetime are larger. Therefore, the deviation of the RG-improved shadow from the classical shadow is larger in the prograde (right) side of the image. Furthermore, this effect grows with increasing spin, see figure 7.

As discussed in section 2.2, the black-hole horizon is no longer spherically symmetric, but instead axisymmetric, in our model. The departure from spherical symmetry is a consequence of the fact that the curvature increases fastest in the equatorial plane, leading to the most pronounced shrinking of the horizon in this plane. This feature also affects the shadow, and can even generate a dent in the shadow if the effects are strong enough, cf. inset of figure 6.
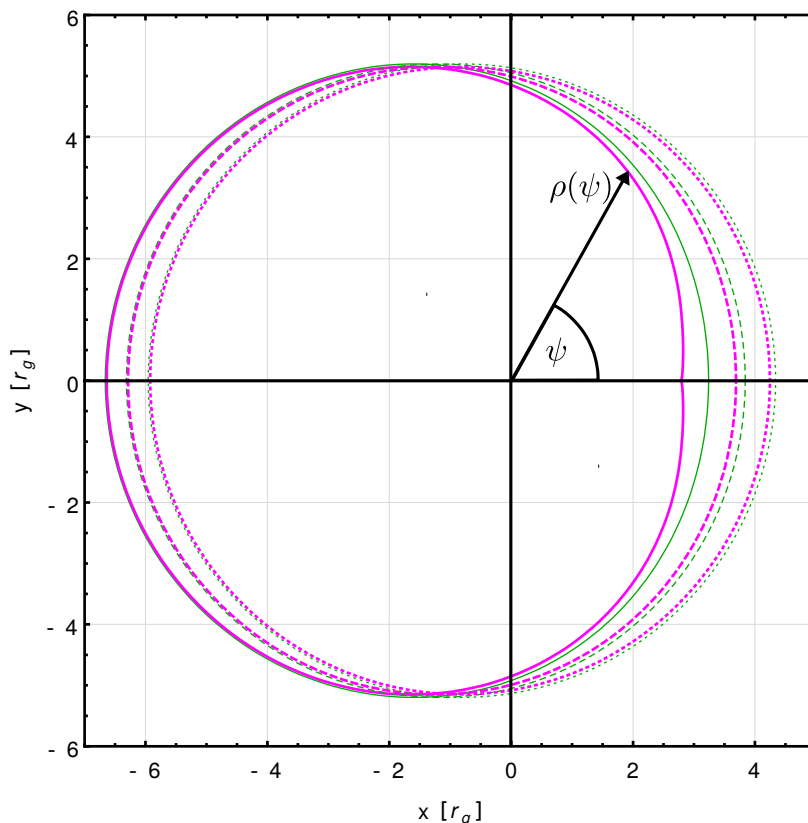
Figure 7. Classical (thin green) and RG-improved (thick magenta) shadows for various spin-parameters $a = 0.4\,r_g$ (dotted), $a = 0.6\,r_g$ (dashed), and $a = 0.8\,r_g$ (continuous). In all cases $\tilde{\gamma} = 0.25$.

In contrast to the spherically symmetric case, the shadow shape of the RG-improved black-hole spacetime is no longer degenerate with a classical shadow shape. Adjusting the two parameters M and a in the classical solution in order to match the two major axes of the RG-improved shadow results in differences at every other point in the image, cf. figure 8. These differences are small and therefore difficult to spatially resolve. Yet, we also point out that comparing the mass at two different radial distances (e.g. extracted from the shadow, and from Keplerian orbits) still allows to distinguish the classical and the RG-improved spacetimes, just as in the spherically symmetric case, at least for sufficiently large $\tilde{\gamma}$.

Next, we explore the image as a function of the inclination i, i.e. the angle between the black hole's spin axis and the line of sight, see figure 9. As one decreases i, the image approaches a circle (just as in the classical Kerr case), and therefore the modifications characteristic of the axisymmetric case become less pronounced.

Overall, the new features in the shadow are most pronounced for fast-spinning black holes viewed from within the equatorial plane, see figure 10. If effects are restricted to the Planck scale, they of course remain too tiny to be detectable — even though modifications are actually always present. We stress that γ can alternatively be viewed as a parameterisation of new, singularity-resolving physics which need not be quantum gravity. In that case, γ is not tied to the Planck scale, and could be significantly larger.

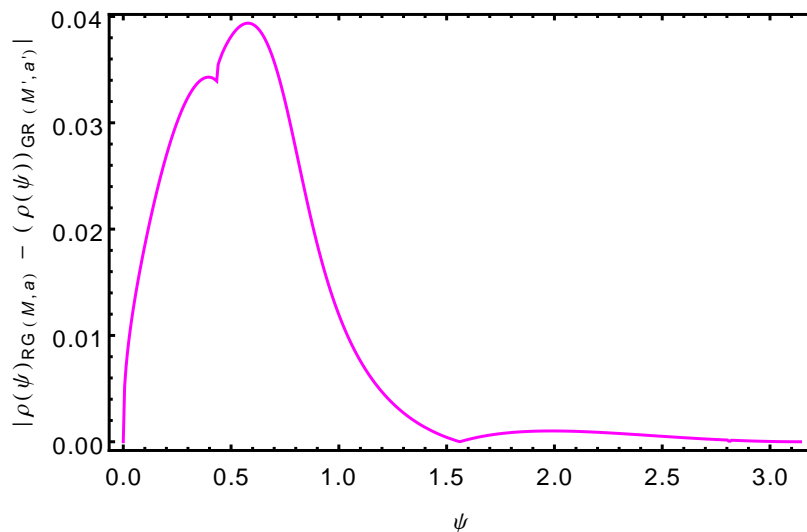**Figure 8**. Difference in radial coordinate of the parameterised shadow boundary $\rho(\psi)$ between the RG-improved shadow (for $M = 1$, $a = 0.99\,r_g$, and $\tilde{\gamma} = 0.008$) and the classical shadow at different mass and spin ($M = 1.001435$, $a = 0.999209\,r_g$). The different mass and spin are chosen such as to result in degenerate points on the major axes at $\psi = 0$, $\pi/2$, π. Every other point on the shadow boundary lifts this degeneracy.

Apart from asymptotic safety, we argue that the effects we describe here could be universal consequences of a large class of quantum-gravity theories. Just as in the Schwarzschild case, one might expect singularity resolution to be tied to an effective weakening of gravity at high curvature scales. Accordingly, the modifications of the black-hole spacetime decrease in magnitude with increasing distance from the horizon. For axisymmetric spacetimes, this has important consequences due to frame-dragging: because of frame-dragging, rays ending up in the prograde (right) side of the picture probe the spacetime much closer to the horizon than in the retrograde (left) side, and are much more affected by the modifications. Accordingly, the shadow is more strongly modified on one side only. Thus, a first rather generic consequence of quantum gravity in spinning spacetimes is that stronger effects are expected on the prograde side. Next, we argue that a dent-like feature in the equatorial plane of the image could also be generic: as the curvature in the classical Kerr spacetime becomes singular only in the equatorial plane, the curvature at fixed radial distance is largest in that plane, resulting in stronger quantum-gravity effects via eq. (2.16). These render the black-hole horizon more compact. Thus, the shadow shrinks more on the prograde side of the picture, and most strongly for $\psi = 0$, compared to the classical case. This is expected to result in a dent-like feature, the extent of which is of course subject to non-universal properties of a given quantum-gravity theory. While these effects are always present, they remain too tiny to be detectable for astrophysical black holes, if the scale of the effect is tied to the Planck scale. An earlier onset of quantum-gravity effects for black holes than expected based on simple power-counting might change this.
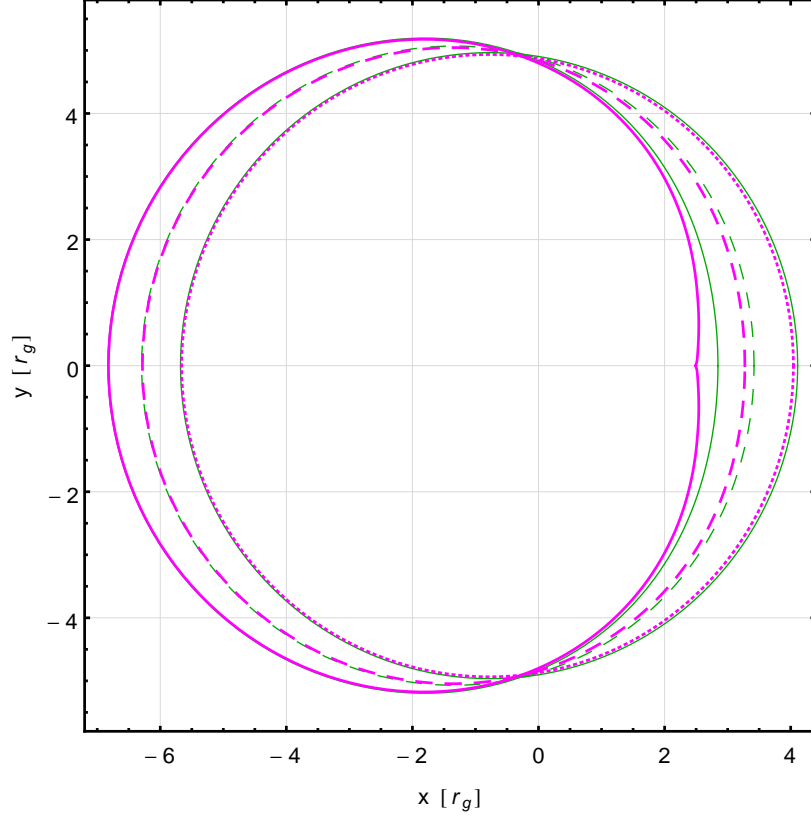
Figure 9. We show the RG improved case (magenta, thick lines) and the classical shadow (green, thin lines) for $a = 0.9\,r_g$ and $\tilde{\gamma} = 0.11$. The angle between the spin axis and the observer is $i = \pi/8$ (dotted lines), $i = \pi/4$ (dashed line) and $i = \pi/2$ (continuous line).
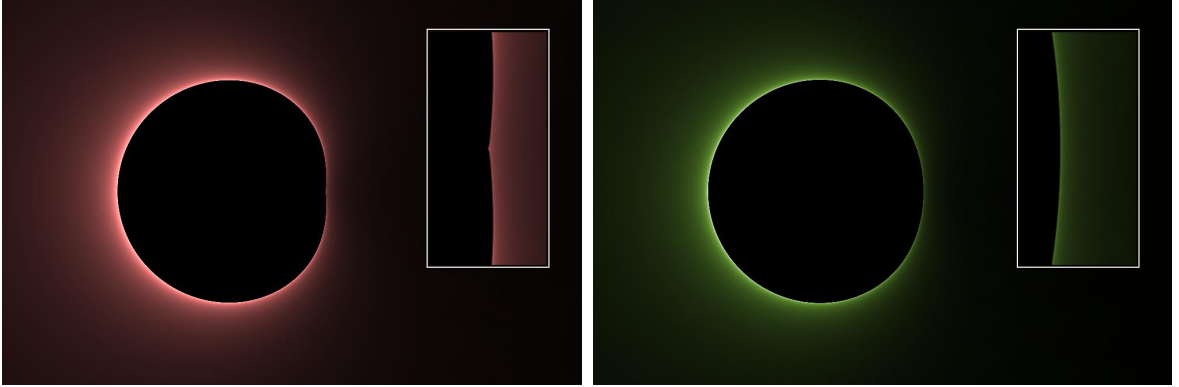

Figure 10. We show the intensity image extracted from the affine-parameter emissivity for an RG-improved (left panel) and classical (right panel), axisymmetric black-hole spacetime with $a = 0.9\,r_g$ and $\tilde{\gamma} = 0.11$. The inset shows a zoom into the prograde (right) side of the image, showing the characteristic dent-like feature in the RG-improved image.

5 Discussion

The groundbreaking observations of the Event Horizon Telescope [38–43] have provided us with a very first image of a black hole. This image opens up a new window into the strong-field regime of gravity, offering a unique possibility to constrain the fundamental physics of spacetime. To confront viable theories of quantum gravity, and more generally singularity-free models, with the observational data now available, resulting features of black-hole shadows have to be derived. We set out to close this gap for asymptotic-safety inspired black-hole spacetimes. A key feature of asymptotically safe gravity is the dynamical weakening of the Newton coupling beyond a critical high-energy scale which is not necessarily tied to the Planck scale. We upgrade classical black-hole spacetimes by incorporating this scale dependence, assuming that the relevant physical scale is the local curvature scale. Therefore, modifications are largest close to the horizon and thus our work is one example of the general point that the shadow size is a powerful test of gravity [95, 120]. In constructing the asymptotic-safety inspired spacetime, we for the first time take into account the angular dependence of the local curvature scale in axisymmetric spacetimes, and add to the evidence that the scale-dependence of the Newton coupling could lead to singularity-resolution.

Let us first highlight the qualitative nature of the resulting effects before commenting on their size. As a consequence of the weakening of gravity at high curvature scales, the upgraded spacetimes we explore feature a more compact horizon. Intuitively, this is a consequence of an effective repulsive force arising due to quantum effects. As our first key result, this leads to a smaller shadow both in the spherically symmetric and axisymmetric case. In the former case, the shadow is degenerate with that of a classical black-hole spacetime of smaller mass. In fact, the asymptotic-safety inspired upgrade of the spherically symmetric spacetime can be parameterised by a mass function depending on the radial distance. This mass function approaches the classical mass from below as a function of increasing distance to the horizon. Therefore, the degeneracy in shadow-size between the classical and upgraded spacetime could be lifted by using a second observable at different radial distance. Specifically, a second mass measurement extracted from Keplerian orbits breaks the degeneracy.

Moreover, there is no degeneracy in spinning spacetimes. Due to frame-dragging, rays arriving at different points in the image plane probe the spacetime at different curvature scales (i.e. different distances to the horizon). In particular, in the near-extremal black-hole case, a subset of light rays probe the spacetime arbitrarily close to the horizon, and are therefore most sensitive to the increased compactness. The latter is most pronounced at the equator of the spinning black hole. Thus, generically, we find that the asymptotic-safety inspired effects put a dent into the shadow close to the equator in the image. Naturally, if quantum-gravity effects are suppressed by the Planck scale, these features are present, but undetectable for astrophysical black holes.

We argue that the two features (the overall shrinking of the shadow and the dent close to the equator) ought to be generic consequences of a large class of quantum-gravity theories. Specifically, we argue that lifting a classical singularity requires an effective repulsive force from quantum gravity. This leads to a more compact black-hole shadow. In the axisymmetric case, we expect this to lead to stronger effects on the flattened side of the shadow, in particular in the equatorial plane. In fact, Loop Quantum Gravity is another example where indications have been found for an effective repulsive character of quantum effects, see, e.g. [12], underlying a scenario for regular black holes [68, 69, 108, 131]. These feature a smaller horizon compared to the classical case, just as in our model. Moreover, a

non-commutative structure of spacetime has also been argued to lead to a regular black-hole spacetime with a smaller horizon than in GR [113]. Further, stringy corrections motivate a similar result [114]. Accordingly, the features we discover here could constitute blueprints for generic quantum-gravity effects.

Within quantum gravity, the most natural scale for the departure from GR to set in, is approximately the Planck scale. Yet, this is based on simple dimensional analysis, and need not hold in a fully dynamical theory. Widening our scope, we point out that singularity-resolution is physically necessary, but need not be tied to quantum gravity, and could be a consequence of new classical physics. Any modification that is equivalent to a repulsive force and thus leads to a de-Sitter-like core, will generically lead to a more compact horizon [53, 54, 74, 85]. In this more general case, the typical scale of modifications becomes a free parameter and our work captures the expected imprints of these modifications on the black-hole shadow. We sketch how observations of the EHT combined with measurements of Keplerian orbits will allow to constrain the free parameter, and motivate an exploration of modified black-hole spacetimes of the form we study here.

To conclude, we highlight that we have computed the shadow for spacetimes which i) feature a horizon, ii) are regular due to a physical mechanism motivated by quantum gravity and iii) are expected to be compatible with the recent groundbreaking observation of the EHT collaboration for the quantum-gravity region of parameter space.

The work presented here serves as a natural stepping stone for a more advanced model that takes into account actual synchrotron emission of relativistic electrons in a turbulent plasma around the black hole as expected for the two main EHT sources Sgr A* and M87*. The behaviour of the plasma can be obtained from General Relativistic Magnetohydrodynamical simulations in the upgraded metric, similar in spirit to [107] yielding four-velocities, densities, temperatures and magnetic field strengths and structures. These predictions then allow evaluations of the synchrotron emissivity enabling to predict images from such models that will carry imprints of the upgraded black-hole spacetime and a direct comparison to data taken by the EHT thereby probing or constraining deviations to GR.

Acknowledgments

A   Error control in Kerr spacetime

Here, we demonstrate how to obtain the minimal required radial distance and numerical precision given a desired error-tolerance in the deflection angle in Kerr spacetime. As a point of reference, we choose the outermost image point $(x, y) = (10\, r_g, 0)$ within the equatorial plane. Within the latter, the deflection angle is exactly calculable with arbitrary precision [90]. Therefore, we use it as a benchmark test for the required numerical precision. Figure 11 shows how the numerical results (blue points) and the exact result (red continuous) develop
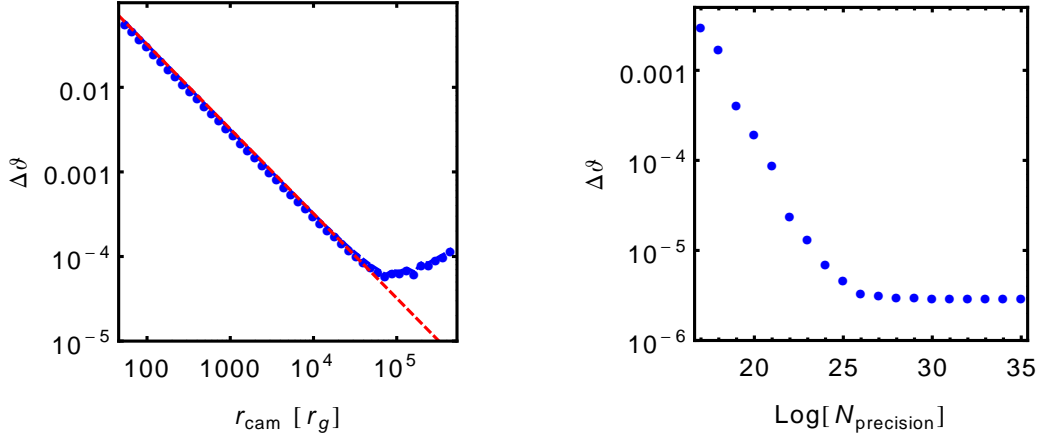
Figure 11. Deflection angle error $\Delta\vartheta = \vartheta_{\text{fit}}(r_{\text{cam}}) - \vartheta$, where ϑ is the exactly calculable deflection angle, as a function of radial camera distance r_{cam} at fixed $N_{\text{precision}} = 10^{-20}$ (left panel) and as a function of numerical precision $N_{\text{precision}}$ at fixed radial camera distance $r_{\text{cam}} = 10^6\, r_g$ (right panel) for $a = 0.99\, r_g$ in classical Kerr spacetime. Blue points show explicit numerical data points. For the radial distance, we also show the fitted function (red dashed), cf. eq. (3.7).
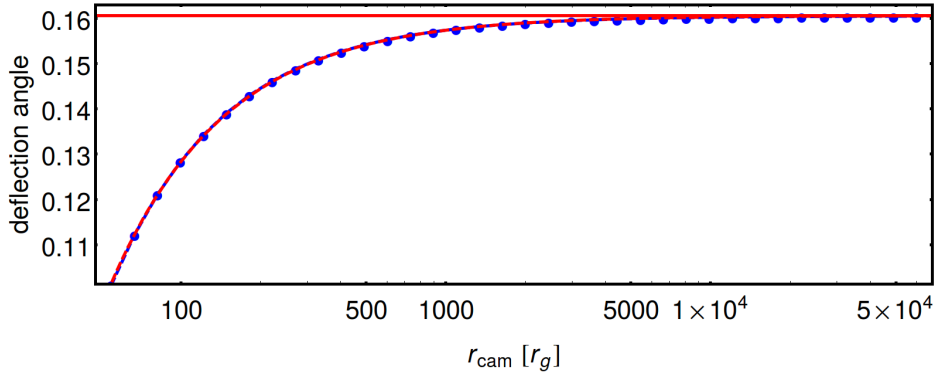

Figure 12. Numerical data (blue connected points), fit (red-dashed) and fitted value ϑ_0, cf. eq. (3.7) (red continuous) for the deflection angle in RG-improved Kerr spacetime with $a = 0.9 r_g$ and $\tilde{\gamma} = 0.11$ at an impact parameter corresponding to the outermost image point $(x, y) = (10, 0)$ in the equatorial plane. The plot shows the dependence on the radial distance r_{cam} at fixed precision $N_{\text{precision}} = 10^{-20}$.

with increasing radial distance and numerical precision. In both plots, we explicitly show how the error convergence stalls due to dominance of the respective other error. In practise, we avoid this by choosing both a large enough camera distance and numerical precision at the same time. Assuming that both errors do not significantly change for the RG-improved metric, we require a maximal error of the deflection angle $\Delta\vartheta = 0.001$ and therefore use $r_{\text{cam}} = 10^4\, r_g$ and $\text{Log}[N_{\text{precision}}] = -20$ throughout all computations. Since the functional form, cf. eq. (3.7), is known, we can test the convergence in radial distance in RG-improved Kerr spacetime explicitly, cf. figure 12.
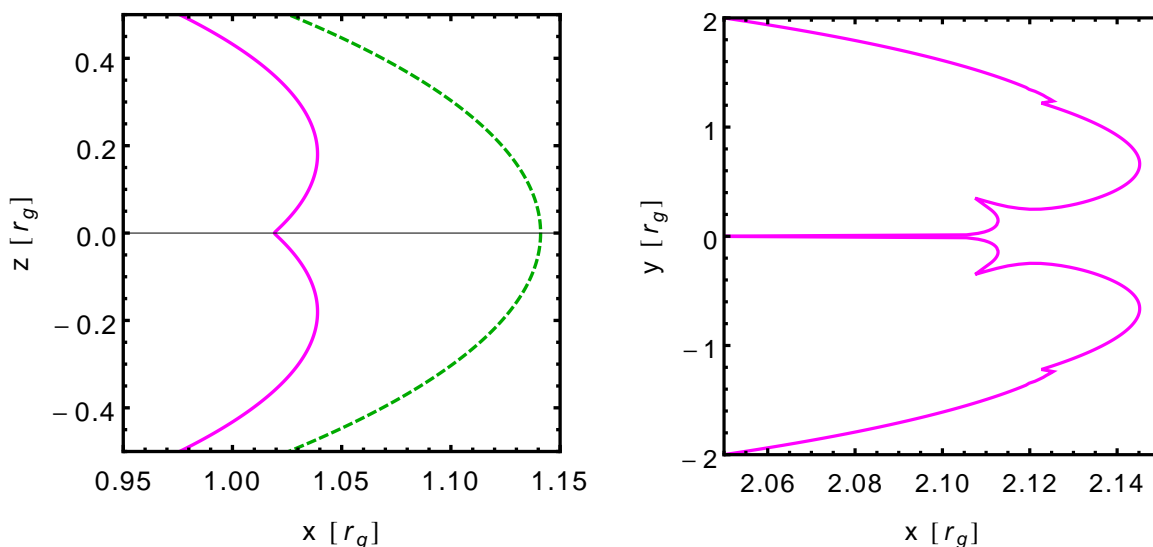
Figure 13. Horizon for the classical and RG-improved Kerr spacetime (left panel) and the RG-improved shadow boundary (right panel) in the equatorial plane for a critical $\tilde{\gamma} = 0.010242$ ($a = 0.99\, r_g$) just before the horizon disappears.

B Features of the shadow for near-critical $\tilde{\gamma}$

Close to critical $\tilde{\gamma}$, the horizon and the resulting shadow image develop additional distinct features. Such features are non-generic in the sense that they only appear for $\tilde{\gamma}$ close to $\tilde{\gamma}_{\text{crit}}$. In the near-critical ($\tilde{\gamma} \approx \tilde{\gamma}_{\text{crit}}$) regime, the dent in the RG-improved horizon at $\theta = \pi/2$ becomes very pronounced, cf. left panel of figure 13. This leads to a more pointy appearance of the dent-like feature in the shadow boundary at $\psi = 0$. Loosely speaking, the horizon takes on the appearance of two largely but not fully overlapping spheres (while remaining differentiable at $\theta = \pi/2$). Further, it results in two sets of distinct, novel features at two intermediate image angles, e.g. for $a = 0.99\, r_g$ and $\tilde{\gamma} \approx \tilde{\gamma}_{\text{crit}} = 0.010242$, these occur at $\psi_{\text{crit},1} \approx \frac{16}{100}\pi$ and $\psi_{\text{crit},2} = \frac{4}{100}\pi$, cf. right panel of figure 13. These secondary features are a consequence of three different regimes for near-horizon null geodesics, cf. figure 14. For $\psi > \psi_{\text{crit},1}$ the light rays closest to the horizon probe the entire horizon. At $|\psi| = \psi_{\text{crit},1}$, the null geodesics transition from wrapping around the entire horizon to wrapping around roughly half of the horizon. Loosely speaking, they probe just one of the two spheres that make up the horizon. Accordingly, the shadow diameter grows significantly at $|\psi| \approx \psi_{\text{crit},1}$. In other words, a smooth, step-like feature appears in the shadow for $|\psi| = \psi_{\text{crit},1}$. As the dent in the shadow is rather prominent for $\tilde{\gamma} \approx \tilde{\gamma}_{\text{crit}}$, it can "trap" trajectories that exist for $|\psi| < \psi_{\text{crit},2}$. As shown in figure 14, these mainly wrap around the dented region of the horizon, and cover a significantly smaller interval in the affine parameter in exploring other parts of the horizon. Accordingly, these probe the smallest values of r of all trajectories, and therefore arrive at values closer to the origin in the image plane.

For less extreme cases, i.e. $\tilde{\gamma} < \tilde{\gamma}_{\text{crit}}$, these features in the shadow-boundary become less pronounced. Nevertheless, traces of these features remain present in the shadow boundary. This can for instance be seen in figure 8 at $\psi \approx 0.4$.

We stress that we do not consider such features universal, in the sense that they can depend on the RG improvement that is used. The existence of the dent in the horizon and shadow, however, is robust.
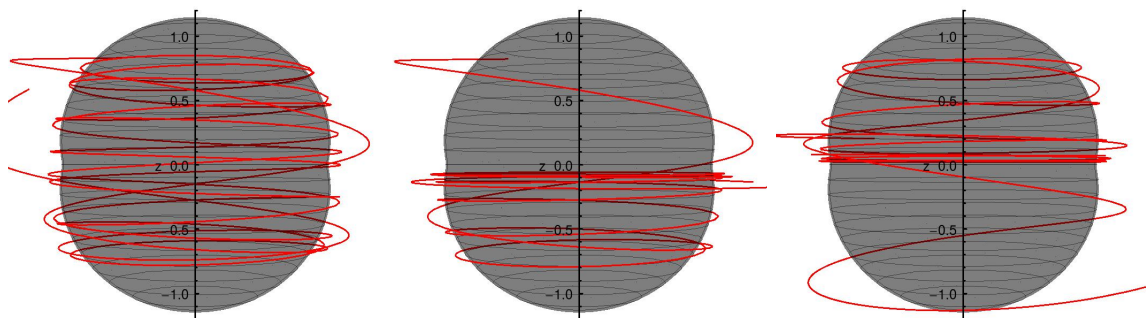
Figure 14. Marginally stable light-like trajectories in the RG-improved black-hole spacetime (thick red lines) for an extreme $\tilde{\gamma} = 0.010242$ ($a = 0.99\,r_g$) just before the horizon (transparent surface) disappears. The left panel shows an image angle $\psi > \psi_{\mathrm{crit},\,1}$. The middle panel shows an image angle $\psi_{\mathrm{crit},\,1} > \psi > \psi_{\mathrm{crit},\,2}$. The right panel shows an image angle $\psi < \psi_{\mathrm{crit},\,2}$.

References

[1] LIGO Scientific and Virgo collaborations, *Observation of Gravitational Waves from a Binary Black Hole Merger*, *Phys. Rev. Lett.* **116** (2016) 061102 [arXiv:1602.03837] [inSPIRE].

[2] LIGO Scientific and Virgo collaborations, *Binary Black Hole Population Properties Inferred from the First and Second Observing Runs of Advanced LIGO and Advanced Virgo*, arXiv:1811.12940 [inSPIRE].

[3] A. Abdujabbarov, M. Amir, B. Ahmedov and S.G. Ghosh, *Shadow of rotating regular black holes*, *Phys. Rev.* **D 93** (2016) 104004 [arXiv:1604.03809] [inSPIRE].

[4] R. Abuter et al., *A geometric distance measurement to the Galactic Center black hole with 0.3% uncertainty*, arXiv:1904.05721.

[5] A. Adeifeoba, A. Eichhorn and A. Platania, *Towards conditions for black-hole singularity-resolution in asymptotically safe quantum gravity*, *Class. Quant. Grav.* **35** (2018) 225007 [arXiv:1808.03472] [inSPIRE].

[6] A. Almheiri, D. Marolf, J. Polchinski and J. Sully, *Black Holes: Complementarity or Firewalls?*, *JHEP* **02** (2013) 062 [arXiv:1207.3123] [inSPIRE].

[7] L. Amarilla, E.F. Eiroa and G. Giribet, *Null geodesics and shadow of a rotating black hole in extended Chern-Simons modified gravity*, *Phys. Rev.* **D 81** (2010) 124045 [arXiv:1005.0607] [inSPIRE].

[8] L. Amarilla and E.F. Eiroa, *Shadow of a rotating braneworld black hole*, *Phys. Rev.* **D 85** (2012) 064019 [arXiv:1112.6349] [inSPIRE].

[9] M. Amir and S.G. Ghosh, *Shapes of rotating nonsingular black hole shadows*, *Phys. Rev.* **D 94** (2016) 024054 [arXiv:1603.06382] [inSPIRE].

[10] GRAVITY collaboration, *Test of the Einstein Equivalence Principle near the Galactic Center Supermassive Black Hole*, *Phys. Rev. Lett.* **122** (2019) 101102 [arXiv:1902.04193] [inSPIRE].

[11] A. Ashtekar, J. Baez, A. Corichi and K. Krasnov, *Quantum geometry and black hole entropy*, *Phys. Rev. Lett.* **80** (1998) 904 [gr-qc/9710007] [inSPIRE].

[12] A. Ashtekar, T. Pawlowski and P. Singh, *Quantum Nature of the Big Bang: An Analytical and Numerical Investigation. I.*, *Phys. Rev.* **D 73** (2006) 124038 [gr-qc/0604013] [inSPIRE].

[13] F. Atamurotov, S.G. Ghosh and B. Ahmedov, *Horizon structure of rotating Einstein-Born-Infeld black holes and shadow*, *Eur. Phys. J.* **C 76** (2016) 273 [arXiv:1506.03690] [ɪɴSPIRE].

[14] D. Ayzenberg and N. Yunes, *Black Hole Shadow as a Test of General Relativity: Quadratic Gravity*, *Class. Quant. Grav.* **35** (2018) 235002 [arXiv:1807.08422] [ɪɴSPIRE].

[15] T. Baker, D. Psaltis and C. Skordis, *Linking Tests of Gravity On All Scales: from the Strong-Field Regime to Cosmology*, *Astrophys. J.* **802** (2015) 63 [arXiv:1412.3455] [ɪɴSPIRE].

[16] C. Bambi and K. Freese, *Apparent shape of super-spinning black holes*, *Phys. Rev.* **D 79** (2009) 043002 [arXiv:0812.1328] [ɪɴSPIRE].

[17] J.M. Bardeen, *Non-singular general-relativistic gravitational collapse*, in *Conference Proceedings of GR5*, Tbilisi, USSR, page 174 (1968).

[18] J.M. Bardeen, *Timelike and null geodesics in the Kerr metric*, in *Black Holes (Les Astres Occlus)*, C. Dewitt and B.S. Dewitt eds., pages 215–239 (1973) [ɪɴSPIRE].

[19] D. Becker and M. Reuter, *En route to Background Independence: Broken split-symmetry and how to restore it with bi-metric average actions*, *Annals Phys.* **350** (2014) 225 [arXiv:1404.4537] [ɪɴSPIRE].

[20] K. Beckwith and C. Done, *Extreme gravitational lensing near rotating black holes*, *Mon. Not. Roy. Astron. Soc.* **359** (2005) 1217 [astro-ph/0411339] [ɪɴSPIRE].

[21] D. Benedetti, P.F. Machado and F. Saueressig, *Asymptotic safety in higher-derivative gravity*, *Mod. Phys. Lett.* **A 24** (2009) 2233 [arXiv:0901.2984] [ɪɴSPIRE].

[22] N.E.J. Bjerrum-Bohr, J.F. Donoghue and B.R. Holstein, *Quantum corrections to the Schwarzschild and Kerr metrics*, *Phys. Rev.* **D 68** (2003) 084005 [*Erratum ibid.* **D 71** (2005) 069904] [hep-th/0211071] [ɪɴSPIRE].

[23] R.D. Blandford and R.L. Znajek, *Electromagnetic extractions of energy from Kerr black holes*, *Mon. Not. Roy. Astron. Soc.* **179** (1977) 433 [ɪɴSPIRE].

[24] A. Bonanno and M. Reuter, *Quantum gravity effects near the null black hole singularity*, *Phys. Rev.* **D 60** (1999) 084011 [gr-qc/9811026] [ɪɴSPIRE].

[25] A. Bonanno and M. Reuter, *Renormalization group improved black hole space-times*, *Phys. Rev.* **D 62** (2000) 043008 [hep-th/0002196] [ɪɴSPIRE].

[26] A. Bonanno and M. Reuter, *Spacetime structure of an evaporating black hole in quantum gravity*, *Phys. Rev.* **D 73** (2006) 083005 [hep-th/0602159] [ɪɴSPIRE].

[27] A. Bonanno, B. Koch and A. Platania, *Cosmic Censorship in Quantum Einstein Gravity*, *Class. Quant. Grav.* **34** (2017) 095012 [arXiv:1610.05299] [ɪɴSPIRE].

[28] A. Bonanno, B. Koch and A. Platania, *Gravitational collapse in Quantum Einstein Gravity*, *Found. Phys.* **48** (2018) 1393 [arXiv:1710.10845] [ɪɴSPIRE].

[29] L. Bosma, B. Knorr and F. Saueressig, *Resolving Spacetime Singularities within Quantum Gravity*, arXiv:1904.04845 [ɪɴSPIRE].

[30] A.E. Broderick, T. Johannsen, A. Loeb and D. Psaltis, *Testing the No-Hair Theorem with Event Horizon Telescope Observations of Sagittarius A**, *Astrophys. J.* **784** (2014) 7 [arXiv:1311.5564] [ɪɴSPIRE].

[31] R. Carballo-Rubio, F. Di Filippo, S. Liberati and M. Visser, *Phenomenological aspects of black holes beyond general relativity*, *Phys. Rev.* **D 98** (2018) 124009 [arXiv:1809.08238] [ɪɴSPIRE].

[32] V. Cardoso and L. Gualtieri, *Testing the black hole 'no-hair' hypothesis*, *Class. Quant. Grav.* **33** (2016) 174001 [arXiv:1607.03133] [ɪɴSPIRE].

[33] B. Carter, *Global structure of the Kerr family of gravitational fields*, *Phys. Rev.* **174** (1968) 1559 [INSPIRE].

[34] A. Cattaneo et al., *The role of black holes in galaxy formation and evolution*, *Nature* **460** (2009) 213 [arXiv:0907.1608] [INSPIRE].

[35] S. Chatzopoulos et al., *The old nuclear star cluster in the Milky Way: dynamics, mass, statistical parallax, and black hole mass*, *Mon. Not. Roy. Astron. Soc.* **447** (2015) 948.

[36] N. Christiansen, K. Falls, J.M. Pawlowski and M. Reichert, *Curvature dependence of quantum gravity*, *Phys. Rev.* **D 97** (2018) 046007 [arXiv:1711.09259] [INSPIRE].

[37] A. Codello, R. Percacci and C. Rahmede, *Investigating the Ultraviolet Properties of Gravity with a Wilsonian Renormalization Group Equation*, *Annals Phys.* **324** (2009) 414 [arXiv:0805.2909] [INSPIRE].

[38] EVENT HORIZON TELESCOPE collaboration, *First M87 Event Horizon Telescope Results. I. The Shadow of the Supermassive Black Hole*, *Astrophys. J.* **875** (2019) L1 [INSPIRE].

[39] EVENT HORIZON TELESCOPE collaboration, *First M87 Event Horizon Telescope Results. II. Array and Instrumentation*, *Astrophys. J.* **875** (2019) L2 [INSPIRE].

[40] EVENT HORIZON TELESCOPE collaboration, *First M87 Event Horizon Telescope Results. III. Data Processing and Calibration*, *Astrophys. J.* **875** (2019) L3 [INSPIRE].

[41] EVENT HORIZON TELESCOPE collaboration, *First M87 Event Horizon Telescope Results. IV. Imaging the Central Supermassive Black Hole*, *Astrophys. J.* **875** (2019) L4 [INSPIRE].

[42] EVENT HORIZON TELESCOPE collaboration, *First M87 Event Horizon Telescope Results. V. Physical Origin of the Asymmetric Ring*, *Astrophys. J.* **875** (2019) L5 [INSPIRE].

[43] EVENT HORIZON TELESCOPE collaboration, *First M87 Event Horizon Telescope Results. VI. The Shadow and Mass of the Central Black Hole*, *Astrophys. J.* **875** (2019) L6 [INSPIRE].

[44] G. Compère, *Are quantum corrections on horizon scale physically motivated?*, arXiv:1902.04504 [INSPIRE].

[45] P.V.P. Cunha and C.A.R. Herdeiro, *Shadows and strong gravitational lensing: a brief review*, *Gen. Rel. Grav.* **50** (2018) 42 [arXiv:1801.00860] [INSPIRE].

[46] P.V.P. Cunha, C.A.R. Herdeiro, E. Radu and H.F. Runarsson, *Shadows of Kerr black holes with scalar hair*, *Phys. Rev. Lett.* **115** (2015) 211102 [arXiv:1509.00021] [INSPIRE].

[47] P.V.P. Cunha, C.A.R. Herdeiro, B. Kleihaus, J. Kunz and E. Radu, *Shadows of Einstein-dilaton-Gauss-Bonnet black holes*, *Phys. Lett.* **B 768** (2017) 373 [arXiv:1701.00079] [INSPIRE].

[48] C.T. Cunningham, *The effects of redshifts and focusing on the spectrum of an accretion disk around a Kerr black hole*, *Astrophys. J.* **202** (1975) 788 [INSPIRE].

[49] M. De Laurentis, Z. Younsi, O. Porth, Y. Mizuno and L. Rezzolla, *Test-particle dynamics in general spherically symmetric black hole spacetimes*, *Phys. Rev.* **D 97** (2018) 104024 [arXiv:1712.00265] [INSPIRE].

[50] J. Dexter and E. Agol, *A Fast New Public Code for Computing Photon Orbits in a Kerr Spacetime*, *Astrophys. J.* **696** (2009) 1616 [arXiv:0903.0620] [INSPIRE].

[51] S. Doeleman et al., *Event-horizon-scale structure in the supermassive black hole candidate at the Galactic Centre*, *Nature* **455** (2008) 78 [arXiv:0809.2442] [INSPIRE].

[52] P. Donà, A. Eichhorn and R. Percacci, *Matter matters in asymptotically safe quantum gravity*, *Phys. Rev.* **D 89** (2014) 084035 [arXiv:1311.2898] [INSPIRE].

[53] I. Dymnikova, *Vacuum nonsingular black hole*, *Gen. Rel. Grav.* **24** (1992) 235 [INSPIRE].

[54] I.G. Dymnikova, *De Sitter-Schwarzschild Black Hole:. its Particlelike Core and Thermodynamical Properties*, *Int. J. Mod. Phys.* **D 5** (1996) 529.

[55] A. Eichhorn, *Status of the asymptotic safety paradigm for quantum gravity and matter*, *Found. Phys.* **48** (2018) 1407 [arXiv:1709.03696] [InSPIRE].

[56] A. Eichhorn, *An asymptotically safe guide to quantum gravity and matter*, *Front. Astron. Space Sci.* **5** (2019) 47 [arXiv:1810.07615] [InSPIRE].

[57] A. Eichhorn and A. Held, *Top mass from asymptotic safety*, *Phys. Lett.* **B 777** (2018) 217 [arXiv:1707.01107] [InSPIRE].

[58] A. Eichhorn and A. Held, *Mass difference for charged quarks from asymptotically safe quantum gravity*, *Phys. Rev. Lett.* **121** (2018) 151302 [arXiv:1803.04027] [InSPIRE].

[59] A. Eichhorn, S. Lippoldt, J.M. Pawlowski, M. Reichert and M. Schiffer, *How perturbative is quantum gravity?*, *Phys. Lett.* **B 792** (2019) 310 [arXiv:1810.02828] [InSPIRE].

[60] E.F. Eiroa and C.M. Sendra, *Shadow cast by rotating braneworld black holes with a cosmological constant*, *Eur. Phys. J.* **C 78** (2018) 91 [arXiv:1711.08380] [InSPIRE].

[61] H. Falcke and S.B. Markoff, *Toward the event horizon — the supermassive black hole in the Galactic Center*, *Class. Quant. Grav.* **30** (2013) 244003 [arXiv:1311.1841] [InSPIRE].

[62] H. Falcke, F. Melia and E. Agol, *Viewing the shadow of the black hole at the galactic center*, *Astrophys. J.* **528** (2000) L13 [astro-ph/9912263] [InSPIRE].

[63] K. Falls, D.F. Litim, K. Nikolakopoulos and C. Rahmede, *A bootstrap towards asymptotic safety*, arXiv:1301.4191 [InSPIRE].

[64] K. Falls and D.F. Litim, *Black hole thermodynamics under the microscope*, *Phys. Rev.* **D 89** (2014) 084002 [arXiv:1212.1821] [InSPIRE].

[65] K. Falls, D.F. Litim and A. Raghuraman, *Black Holes and Asymptotically Safe Gravity*, *Int. J. Mod. Phys.* **A 27** (2012) 1250019 [arXiv:1002.0260] [InSPIRE].

[66] K.G. Falls, D.F. Litim and J. Schröder, *Aspects of asymptotic safety for quantum gravity*, arXiv:1810.08550 [InSPIRE].

[67] L. Fidkowski, V. Hubeny, M. Kleban and S. Shenker, *The Black hole singularity in AdS/CFT*, *JHEP* **02** (2004) 014 [hep-th/0306170] [InSPIRE].

[68] R. Gambini and J. Pullin, *Black holes in loop quantum gravity: The Complete space-time*, *Phys. Rev. Lett.* **101** (2008) 161301 [arXiv:0805.1187] [InSPIRE].

[69] R. Gambini and J. Pullin, *Loop quantization of the Schwarzschild black hole*, *Phys. Rev. Lett.* **110** (2013) 211301 [arXiv:1302.5265] [InSPIRE].

[70] J.P. Gauntlett, R.C. Myers and P.K. Townsend, *Black holes of $D = 5$ supergravity*, *Class. Quant. Grav.* **16** (1999) 1 [hep-th/9810204] [InSPIRE].

[71] K. Gebhardt et al., *The Black-Hole Mass in M87 from Gemini/NIFS Adaptive Optics Observations*, *Astrophys. J.* **729** (2011) 119 [arXiv:1101.1954] [InSPIRE].

[72] A.M. Ghez, B.L. Klein, M. Morris and E.E. Becklin, *High proper motion stars in the vicinity of Sgr A*: Evidence for a supermassive black hole at the center of our galaxy*, *Astrophys. J.* **509** (1998) 678 [astro-ph/9807210] [InSPIRE].

[73] A.M. Ghez et al., *Measuring Distance and Properties of the Milky Way's Central Supermassive Black Hole with Stellar Orbits*, *Astrophys. J.* **689** (2008) 1044 [arXiv:0808.2870] [InSPIRE].

[74] S.G. Ghosh, *A nonsingular rotating black hole*, *Eur. Phys. J.* **C 75** (2015) 532 [arXiv:1408.5668] [InSPIRE].

[75] S.B. Giddings, *Astronomical tests for quantum black hole structure*, *Nat. Astron.* **1** (2017) 0067 [arXiv:1703.03387] [InSPIRE].

[76] S.B. Giddings, S. Koren and G. Treviño, *Exploring strong-field deviations from general relativity via gravitational waves*, arXiv:1904.04258 [INSPIRE].

[77] H. Gies, B. Knorr, S. Lippoldt and F. Saueressig, *Gravitational Two-Loop Counterterm Is Asymptotically Safe*, *Phys. Rev. Lett.* **116** (2016) 211302 [arXiv:1601.01800] [INSPIRE].

[78] S. Gillessen et al., *Monitoring stellar orbits around the Massive Black Hole in the Galactic Center*, *Astrophys. J.* **692** (2009) 1075 [arXiv:0810.4674] [INSPIRE].

[79] R. Gold, J.C. McKinney, M.D. Johnson and S.S. Doeleman, *Probing the Magnetic Field Structure in* Sgr A∗ *on Black Hole Horizon Scales with Polarized Radiative Transfer Simulations*, *Astrophys. J.* **837** (2017) 180 [arXiv:1601.05550] [INSPIRE].

[80] M.H. Goroff and A. Sagnotti, *Quantum gravity at two loops*, *Phys. Lett.* **160B** (1985) 81 [INSPIRE].

[81] GRAVITY collaboration, *Detection of the gravitational redshift in the orbit of the star S2 near the Galactic centre massive black hole*, *Astron. Astrophys.* **615** (2018) L15 [arXiv:1807.09409] [INSPIRE].

[82] GRAVITY collaboration, *Detection of orbital motions near the last stable circular orbit of the massive black hole SgrA**, *Astron. Astrophys.* **618** (2018) L10 [arXiv:1810.12641].

[83] A. Grenzebach, V. Perlick and C. Lämmerzahl, *Photon Regions and Shadows of Kerr-Newman-NUT Black Holes with a Cosmological Constant*, *Phys. Rev.* **D 89** (2014) 124004 [arXiv:1403.5234] [INSPIRE].

[84] H.M. Haggard and C. Rovelli, *Quantum Gravity Effects around Sagittarius A**, *Int. J. Mod. Phys.* **D 25** (2016) 1644021 [arXiv:1607.00364] [INSPIRE].

[85] S.A. Hayward, *Formation and evaporation of regular black holes*, *Phys. Rev. Lett.* **96** (2006) 031103 [gr-qc/0506126] [INSPIRE].

[86] S. He and D. Rideout, *A Causal Set Black Hole*, *Class. Quant. Grav.* **26** (2009) 125015 [arXiv:0811.4235] [INSPIRE].

[87] A. Held, R. Gold and A. Eichhorn, *Black-hole shadow in higher-derivative gravity*, to appear (2019).

[88] D. Hilbert, *Nachrichten von der Königlichen Gesellschaft der Wissenschaften zu Göttingen — Mathematisch-physikalische Klasse*, chapter Die Grundlagen der Physik — Zweite Mitteilung, pages 53–76, Weidmannsche Buchhandlung, Berlin (1917).

[89] G.T. Horowitz and S.F. Ross, *Possible resolution of black hole singularities from large N gauge theory*, *JHEP* **04** (1998) 015 [hep-th/9803085] [INSPIRE].

[90] S.V. Iyer and E.C. Hansen, *Light's Bending Angle in the Equatorial Plane of a Kerr Black Hole*, *Phys. Rev.* **D 80** (2009) 124023 [arXiv:0907.5352] [INSPIRE].

[91] T. Johannsen, *Regular Black Hole Metric with Three Constants of Motion*, *Phys. Rev.* **D 88** (2013) 044002 [arXiv:1501.02809] [INSPIRE].

[92] T. Johannsen, *Sgr A* and General Relativity*, *Class. Quant. Grav.* **33** (2016) 113001 [arXiv:1512.03818] [INSPIRE].

[93] T. Johannsen, *Testing the No-Hair Theorem with Observations of Black Holes in the Electromagnetic Spectrum*, *Class. Quant. Grav.* **33** (2016) 124001 [arXiv:1602.07694] [INSPIRE].

[94] T. Johannsen and D. Psaltis, *Testing the No-Hair Theorem with Observations in the Electromagnetic Spectrum: II. Black-Hole Images*, *Astrophys. J.* **718** (2010) 446 [arXiv:1005.1931] [INSPIRE].

[95] T. Johannsen et al., *Testing General Relativity with the Shadow Size of Sgr A**, *Phys. Rev. Lett.* **116** (2016) 031101 [arXiv:1512.02640] [INSPIRE].

[96] D.J. Kapner et al., *Tests of the gravitational inverse-square law below the dark-energy length scale*, *Phys. Rev. Lett.* **98** (2007) 021101 [hep-ph/0611184] [ɪɴSPIRE].

[97] B. Koch and F. Saueressig, *Structural aspects of asymptotically safe black holes*, *Class. Quant. Grav.* **31** (2014) 015006 [arXiv:1306.1546] [ɪɴSPIRE].

[98] B. Koch and F. Saueressig, *Black holes within Asymptotic Safety*, *Int. J. Mod. Phys.* **A 29** (2014) 1430011 [arXiv:1401.4452] [ɪɴSPIRE].

[99] G. Kofinas and V. Zarikas, *Avoidance of singularities in asymptotically safe Quantum Einstein Gravity*, *JCAP* **10** (2015) 069 [arXiv:1506.02965] [ɪɴSPIRE].

[100] R. Konoplya, L. Rezzolla and A. Zhidenko, *General parametrization of axisymmetric black holes in metric theories of gravity*, *Phys. Rev.* **D 93** (2016) 064015 [arXiv:1602.02378] [ɪɴSPIRE].

[101] O. Lauscher and M. Reuter, *Ultraviolet fixed point and generalized flow equation of quantum gravity*, *Phys. Rev.* **D 65** (2002) 025013 [hep-th/0108040] [ɪɴSPIRE].

[102] D.F. Litim, *Fixed points of quantum gravity*, *Phys. Rev. Lett.* **92** (2004) 201301 [hep-th/0312114] [ɪɴSPIRE].

[103] D.F. Litim and K. Nikolakopoulos, *Quantum gravity effects in Myers-Perry space-times*, *JHEP* **04** (2014) 021 [arXiv:1308.5630] [ɪɴSPIRE].

[104] J.P. Luminet, *Image of a spherical black hole with thin accretion disk*, *Astron. Astrophys.* **75** (1979) 228 [ɪɴSPIRE].

[105] E. Manrique, S. Rechenberger and F. Saueressig, *Asymptotically Safe Lorentzian Gravity*, *Phys. Rev. Lett.* **106** (2011) 251302 [arXiv:1102.5012] [ɪɴSPIRE].

[106] L. Meyer et al., *The Shortest Known Period Star Orbiting our Galaxy's Supermassive Black Hole*, *Science* **338** (2012) 84 [arXiv:1210.1294] [ɪɴSPIRE].

[107] Y. Mizuno et al., *The Current Ability to Test Theories of Gravity with Black Hole Shadows*, *Nat. Astron.* **2** (2018) 585 [arXiv:1804.05812] [ɪɴSPIRE].

[108] L. Modesto, *Semiclassical loop quantum black hole*, *Int. J. Theor. Phys.* **49** (2010) 1649 [arXiv:0811.2196] [ɪɴSPIRE].

[109] J.W. Moffat, *Modified Gravity Black Holes and their Observable Shadows*, *Eur. Phys. J.* **C 75** (2015) 130 [arXiv:1502.01677] [ɪɴSPIRE].

[110] J.R. Mureika and G.U. Varieschi, *Black hole shadows in fourth-order conformal Weyl gravity*, *Can. J. Phys.* **95** (2017) 1299 [arXiv:1611.00399] [ɪɴSPIRE].

[111] P. Nicolini, *Noncommutative nonsingular black holes*, *Bled Workshops Phys.* **6** (2005) 79 [hep-th/0510203] [ɪɴSPIRE].

[112] P. Nicolini, *Noncommutative Black Holes, The Final Appeal To Quantum Gravity: A Review*, *Int. J. Mod. Phys.* **A 24** (2009) 1229 [arXiv:0807.1939] [ɪɴSPIRE].

[113] P. Nicolini, A. Smailagic and E. Spallucci, *Noncommutative geometry inspired Schwarzschild black hole*, *Phys. Lett.* **B 632** (2006) 547 [gr-qc/0510112] [ɪɴSPIRE].

[114] P. Nicolini, E. Spallucci and M.F. Wondrak, *Quantum Corrected Black Holes from String T-duality*, arXiv:1902.11242 [ɪɴSPIRE].

[115] M. Okounkova, M.A. Scheel and S.A. Teukolsky, *Numerical black hole initial data and shadows in dynamical Chern-Simons gravity*, *Class. Quant. Grav.* **36** (2019) 054001 [arXiv:1810.05306] [ɪɴSPIRE].

[116] J.M. Pawlowski and D. Stock, *Quantum-improved Schwarzschild-(A)dS and Kerr-(A)dS spacetimes*, *Phys. Rev.* **D 98** (2018) 106008 [arXiv:1807.10512] [ɪɴSPIRE].

[117] R. Percacci, *An Introduction to Covariant Quantum Gravity and Asymptotic Safety, 100 Years of General Relativity*, volume 3 World Scientific (2017).

[118] A. Platania, *Dynamical renormalization of black-hole spacetimes*, *Eur. Phys. J.* **C 79** (2019) 470 [arXiv:1903.10411] [INSPIRE].

[119] F. Pretorius, *Binary Black Hole Coalescence*, *Astrophys. Space Sci. Libr.* **305** (2009) 359.

[120] D. Psaltis, *Testing General Relativity with the Event Horizon Telescope*, arXiv:1806.09740 [INSPIRE].

[121] D. Psaltis, F. Ozel, C.-K. Chan and D.P. Marrone, *A General Relativistic Null Hypothesis Test with Event Horizon Telescope Observations of the black-hole shadow in Sgr A**, *Astrophys. J.* **814** (2015) 115 [arXiv:1411.1454] [INSPIRE].

[122] N. Sridhar, S. Bhattacharyya, S. Chandra and H.M. Antia, *Broadband reflection spectroscopy of MAXI J1535-571 using AstroSat: Estimation of black hole mass and spin*, arXiv:1905.09253 [INSPIRE].

[123] M. Reuter, *Nonperturbative evolution equation for quantum gravity*, *Phys. Rev.* **D 57** (1998) 971 [hep-th/9605030] [INSPIRE].

[124] M. Reuter and F. Saueressig, *Renormalization group flow of quantum gravity in the Einstein-Hilbert truncation*, *Phys. Rev.* **D 65** (2002) 065016 [hep-th/0110054] [INSPIRE].

[125] M. Reuter and E. Tuiran, *Quantum Gravity Effects in Rotating Black Holes*, in *Recent developments in theoretical and experimental general relativity, gravitation and relativistic field theories. Proceedings, 11th Marcel Grossmann Meeting, MG11*, Berlin, Germany, July 23–29, 2006, Pt. A-C, pp. 2608–2610 (2006) [DOI:10.1142/9789812834300_0473] [hep-th/0612037] [INSPIRE].

[126] M. Reuter and E. Tuiran, *Quantum Gravity Effects in the Kerr Spacetime*, *Phys. Rev.* **D 83** (2011) 044041 [arXiv:1009.3528] [INSPIRE].

[127] M. Reuter and F. Saueressig, *Quantum Gravity and the Functional Renormalization Group*, Cambridge University Press (2019) [INSPIRE].

[128] C.S. Reynolds, *Measuring Black Hole Spin using X-ray Reflection Spectroscopy*, *Space Sci. Rev.* **183** (2014) 277 [arXiv:1302.3260] [INSPIRE].

[129] C.S. Reynolds and M.A. Nowak, *Fluorescent iron lines as a probe of astrophysical black hole systems*, *Phys. Rept.* **377** (2003) 389 [astro-ph/0212065] [INSPIRE].

[130] L. Rezzolla and A. Zhidenko, *New parametrization for spherically symmetric black holes in metric theories of gravity*, *Phys. Rev.* **D 90** (2014) 084009 [arXiv:1407.3086] [INSPIRE].

[131] C. Rovelli and F. Vidotto, *Planck stars*, *Int. J. Mod. Phys.* **D 23** (2014) 1442026 [arXiv:1401.6562] [INSPIRE].

[132] M. Shaposhnikov and C. Wetterich, *Asymptotic safety of gravity and the Higgs boson mass*, *Phys. Lett.* **B 683** (2010) 196 [arXiv:0912.0208] [INSPIRE].

[133] Z. Stuchlík and J. Schee, *Shadow of the regular Bardeen black holes and comparison of the motion of photons and neutrinos*, *Eur. Phys. J.* **C 79** (2019) 44 [INSPIRE].

[134] G. 't Hooft, *On the Quantum Structure of a Black Hole*, *Nucl. Phys.* **B 256** (1985) 727 [INSPIRE].

[135] G. 't Hooft and M.J.G. Veltman, *One loop divergencies in the theory of gravitation*, *Ann. Inst. H. Poincare Phys. Theor.* **A 20** (1974) 69 [INSPIRE].

[136] R. Torres, *Singularity-free gravitational collapse and asymptotic safety*, *Phys. Lett.* **B 733** (2014) 21 [arXiv:1404.7655] [INSPIRE].

[137] R. Torres and F. Fayos, *On the quantum corrected gravitational collapse*, *Phys. Lett.* **B 747** (2015) 245 [arXiv:1503.07407] [INSPIRE].

[138] N. Tsukamoto, *Black hole shadow in an asymptotically-flat, stationary and axisymmetric spacetime: The Kerr-Newman and rotating regular black holes*, *Phys. Rev.* **D 97** (2018) 064021 [arXiv:1708.07427] [INSPIRE].

[139] A.E.M. van de Ven, *Two loop quantum gravity*, *Nucl. Phys.* **B 378** (1992) 309 [INSPIRE].

[140] T. Vetsov, G. Gyulchev and S. Yazadjiev, *Shadows of Black Holes in Vector-Tensor Galileons Modified Gravity*, arXiv:1801.04592 [INSPIRE].

[141] S.U. Viergutz, *Image generation in Kerr geometry. I. Analytical investigations on the stationary emitter-observer problem*, *Astron. Astrophys.* **272** (1993) 355.

[142] F.H. Vincent, E. Gourgoulhon, C. Herdeiro and E. Radu, *Astrophysical imaging of Kerr black holes with scalar hair*, *Phys. Rev.* **D 94** (2016) 084045 [arXiv:1606.04246] [INSPIRE].

[143] M. von Laue, *Die Relativitätstheorie*, Vol. 1: *Das Relativitätsprinzip der Lorentztransformation*, Vol. 2: *Die allgemeine Relativitätstheorie und Einsteins Lehre von der Schwerkraft*, Friedrich Vieweg & Sohn, Braunschweig (1921).

[144] J.L. Walsh, A.J. Barth, L.C. Ho and M. Sarzi, *The M87 Black Hole Mass from Gas-dynamical Models of Space Telescope Imaging Spectrograph Observations*, *Astrophys. J.* **770** (2013) 86 [arXiv:1304.7273] [INSPIRE].

[145] H.-M. Wang, Y.-M. Xu and S.-W. Wei, *Shadows of Kerr-like black holes in a modified gravity theory*, *JCAP* **03** (2019) 046 [arXiv:1810.12767] [INSPIRE].

[146] S.-W. Wei and Y.-X. Liu, *Observing the shadow of Einstein-Maxwell-Dilaton-Axion black hole*, *JCAP* **11** (2013) 063 [arXiv:1311.4251] [INSPIRE].

[147] S.-W. Wei, P. Cheng, Y. Zhong and X.-N. Zhou, *Shadow of noncommutative geometry inspired black hole*, *JCAP* **08** (2015) 004 [arXiv:1501.06298] [INSPIRE].

[148] N.N. Weinberg, M. Milosavljevic and A.M. Ghez, *Stellar dynamics at the Galactic Center with a Thirty Meter Telescope*, *Astrophys. J.* **622** (2005) 878 [astro-ph/0404407] [INSPIRE].

[149] S. Weinberg, *Ultraviolet divergences in quantum theories of gravitation*, in *General Relativity: An Einstein centenary survey*, S.W. Hawking, and W. Israel eds., Cambridge University Press, pages 790–831 (1979) [INSPIRE].

[150] C.M. Will, *The Confrontation between General Relativity and Experiment*, *Living Rev. Rel.* **17** (2014) 4 [arXiv:1403.7377] [INSPIRE].

[151] Inc. Wolfram Research, *Mathematica*, version 11.2, Champaign, Illinois (2017).

[152] Z. Younsi, A. Zhidenko, L. Rezzolla, R. Konoplya and Y. Mizuno, *New method for shadow calculations: Application to parametrized axisymmetric black holes*, *Phys. Rev.* **D 94** (2016) 084025 [arXiv:1607.05767] [INSPIRE].